Environmental Context for the Terminal Ediacaran Biomineralization of Animals

Short running title: **Environmental context for animal biomineralization**

H. CUI,[1,2,*] A. J. KAUFMAN,[1,3] S. XIAO,[4] S. PEEK,[1,†] H. CAO,[1,‡] X. MIN,[5] Y. CAI,[5] Z. SIEGEL,[6] X.-M. LIU,[7] Y. PENG,[8] J. D. SCHIFFBAUER,[9] AND A. J. MARTIN,[10]

[1] Department of Geology, University of Maryland, College Park, MD, 20742, USA
[2] Department of Geoscience and NASA Astrobiology Institute, University of Wisconsin-Madison, WI, 53706, USA
[3] Earth System Science Interdisciplinary Center, University of Maryland, College Park, MD, 20742, USA
[4] Department of Geosciences, Virginia Tech, Blacksburg, VA 24061, USA
[5] Department of Geology, Northwest University, Xi'an 710069, China
[6] Bethesda-Chevy Chase High School, Bethesda, MD, 20814, USA
[7] Department of Geological Sciences, University of North Carolina, Chapel Hill, NC 27599-3315
[8] Department of Geology and Geophysics, Louisiana State University, Baton Rouge, LA 70803, USA
[9] Department of Geological Sciences, University of Missouri, Columbia, Missouri 65211, USA
[10] División de Geociencias Aplicadas, IPICYT, San Luis Potosí 78216, Mexico

[*]Corresponding author: Huan.Cui@wisc.edu (H. Cui) Fax: +1 608 262 0693
[†] Present address: United States Geological Survey, Menlo Park, CA 94025, USA
[‡] Present address: College of Earth Sciences, Jilin University, Changchun 130061, China

ABSTRACT

In terminal Ediacaran strata of South China, the onset of calcareous biomineralization is preserved in the paleontological transition from *Conotubus* to *Cloudina* in repetitious limestone facies of the Dengying Formation. Both fossils have similar size, funnel-in-funnel construction, and epibenthic lifestyle, but *Cloudina* is biomineralized whereas *Conotubus* is not. To provide environmental context for this evolutionary milestone, we conducted a high-resolution elemental and stable isotope study of the richly fossiliferous Gaojiashan Member. Coincident with the first appearance of *Cloudina* is a significant positive carbonate carbon isotope excursion (up to +6‰) and an increase in the abundance and ^{34}S composition of pyrite. In contrast, $\delta^{34}S$ values of carbonate-associated sulfate (CAS) remain steady throughout the succession, resulting in anomalously large (>70‰) sulfur isotope fractionations in the lower half of the member. The fractionation trend likely relates to changes in microbial communities, with sulfur disproportionation involved in the lower interval whereas microbial sulfate reduction was the principal metabolic pathway in the upper. We speculate that the coupled paleontological and biogeochemical anomalies may have coincided with an increase in terrestrial weathering fluxes of sulfate, alkalinity, and nutrients to the depositional basin, which stimulated primary productivity, the spread of an oxygen minimum zone, and the development of euxinic conditions in subtidal and basinal environments. Enhanced production and burial of organic matter is thus directly connected to the carbon isotope anomaly, and likely promoted pyritization as the main taphonomic pathway for *Conotubus* and other soft-bodied Ediacara biotas. Our studies suggest that the Ediacaran confluence of ecological pressures from predation and environmental pressures from an increase in seawater alkalinity set the stage for an unprecedented geobiological response: the evolutionary novelty of animal biomineralization.

INTRODUCTION

One of the earliest animals to have developed a biomineralized carbonate exoskeleton is *Cloudina* — named after the famed Precambrian paleontologist Preston Cloud (1912–1991) and preserved in terminal Ediacaran (ca. 550–541 Ma) sedimentary successions worldwide (Conway Morris et al., 1990; Sour-Tovar et al., 2007; Gaucher and Germs, 2009; Cortijo et al., 2010; Zhuravlev et al., 2012). This animal, which is suggested to be an ancient cnidarian-grade (Grant, 1992; Cortijo et al., 2010) or lophotrochozoan animal (Hua et al., 2005; Zhuravlev et al., 2015), constructed a high-Mg calcitic tubular shell with nested funnels, had an epibenthic lifestyle with its apex attached to the substrate (Grant, 1990; Zhuravlev et al., 2012; Cai et al., 2014), and may have had both sexual and asexual reproductive strategies to aid in its broad ecological dispersal

(Cortijo et al., 2015). *Cloudina* was associated with microbial reefs, and may have been a reef builder like modern-day corals that inhabit oligotrophic shelf environments where they band together in search of hard substrates and for protection against predators (Penny et al., 2014; Wood and Curtis, 2015).

Biomineralization of *Cloudina* is widely considered to have been a response to predation given the significant number of borings found on its fossil shells (Bengtson and Zhao, 1992; Hua et al., 2003; Porter, 2011). In addition, some also have considered terminal Ediacaran biomineralization as a (toxico-)physiological response to regulate calcium concentrations in circulatory fluids (Simkiss, 1977; Kempe et al., 1989; Simkiss, 1989; Brennan et al., 2004), or to environmental perturbations involving oscillations in atmospheric pCO_2 and seawater chemistry (Knoll, 2003a; Knoll and Fischer, 2011). Environmental drivers, however, are particularly difficult to assess insofar as these should also have a broad effect on general biotic diversification and vice versa (Knoll, 2003b; Gaidos et al., 2007; Butterfield, 2009; Butterfield, 2011; Lenton et al., 2014; Erwin, 2015). Insofar as there is a metabolic cost to biomineralization, the biological benefits to the organisms, including protection against predation and the physiological response of organisms to rapidly changing seawater chemistry in the terminal Ediacaran Period, should be balanced (Knoll, 2003a; Xiao, 2014).

To this end, we investigated a Lagerstätte of Ediacaran animals in the Gaojiashan Member of the Dengying Formation in South China (**Fig. 1**) (Hua et al., 2007; Cai et al., 2010). Within the member's repetitious limestone facies, the first appearance of *Cloudina* is immediately preceded by *Conotubus*, a soft-bodied antecedent exquisitely preserved through pyritization with similar construction, size, and lifestyle (Cai et al., 2011; Cai et al., 2014). To explore this unique paleontological juxtaposition and provide environmental context for the earliest examples of animal biomineralization and pyritization, we sampled the Gaojiashan Member at high stratigraphic resolution for elemental and isotopic compositions. Our chemostratigraphic investigation reveals that these evolutionary and taphonomic events are associated with profound biogeochemical shifts in both the carbon and sulfur cycles, and speculate that they may have been facilitated by profound environmental perturbations in the marine realm ultimately driven by enhanced oxidative weathering of the continents.

METHODS

In this study, the Gaojiashan Member was systematically sampled at high resolution for integrated chemostratigraphic and geochronological investigations. Geochemical analyses were conducted in the Paleoclimate CoLaboratory at University of Maryland. Details of the methods used in the CoLaboratory can be found in previous publications (e.g. McFadden et al., 2008; Zhelezinskaia et al., 2014; Cui et al., 2015), but are briefly outlined below.

Carbon and oxygen isotope analysis

Rock samples were cut and polished for detailed petrographic observation and micro-drilling in order to obtain powders from the least-altered, least-recrystallized, and purest phases for carbonate carbon ($\delta^{13}C_{carb}$) and oxygen ($\delta^{18}O_{carb}$) isotope analysis. The powders were measured with a Multicarb inlet device in-line with an Elementar Isoprime continuous-flow isotope ratio mass spectrometer, and precision for both isotopes was routinely better than 0.1‰.

Elemental analyses

Major and trace elemental abundances in carbonates were analyzed in order to better evaluate the degree of diagenetic alteration. Aliquots of the micro-drilled carbonate powders were dissolved in 0.4 M HNO_3, centrifuged, and only analyzed for the solutions. Petrographic observations indicate that these powders were largely free of siliciclastics; any clays, if present, would not have been dissolved by the dilute acid. The resulting solutions were analyzed on a Thermo Scientific® iCAP-Q ICP-MS (Inductively Coupled Plasma – Mass Spectrometry) at the Carnegie Institution of Washington. Precision of these analyses as determined by repeated measurements of a house standard carbonate was < 5% (2σ) for major elements with high concentrations and < 10% (2σ) for the REEs.

Orgnic carbon and paired sulfur isotope analyses

The organic carbon ($\delta^{13}C_{org}$), total sulfur ($\delta^{34}S_{TS}$ of pyrite and trace amount of organic S) isotope compositions were measured by combustion of the decalcified residuals to CO_2 or SO_2 with a Eurovector elemental analyzer in-line with a second Elementar Isoprime isotope ratio mass spectrometer. Bulk carbonate powders were used for extraction of carbonate-associated sulfate (CAS). For the former, ~15 g of bulk crushed sample was acidified with 3 M HCl. These acidified residues were washed with ultra-pure Milli-Q (18MΩ) water, centrifuged, decanted, and dried. For the latter, ~100 g of crushed bulk sample, which were repeatedly leached with 10% NaCl solutions. To minimize the contamination of soluble non-CAS sulfate (Marenco et al., 2008; Wotte et al., 2012; Peng et al., 2014; Schobben et al., 2015), bulk powders were leached by 10% NaCl solutions for at least 10 times with at least two hours for each time, and then washed with Milli-Q water for at least 3 times prior to acidification of the leached powders with 3 M HCl. CAS precipitates were then collected as $BaSO_4$ three days after $BaCl_2$ was added to the solution. The residues and the $BaSO_4$ precipitates were packed into folded tin cups with V_2O_5 for combustion to CO_2 or SO_2 in a Eurovector elemental analyzer in-line with a second Elementar Isoprime isotope ratio mass spectrometer, which measured isotope abundances. Uncertainties for carbon and sulfur isotope measurements determined by multiple analyses of standard materials during analytical sessions are better than 0.1% and 0.3‰, respectively.

Detrital zircon dating

For all aspects of zircon dating we followed the procedures described in Martin et al. (2015). Zircon grains were isolated using conventional mineral separation techniques including rock pulverization by hand using a mortar and pestle, removal of silt and clay by hand panning in water, removal of magnetic grains using a Frantz magnetic barrier separator, and density separation using methylene iodide. Zircon grains were then poured onto double-sided tape and cast them in an epoxy disk along with approximately 10 shards of the Sri Lanka zircon standard (564±3 Ma) (Gehrels et al., 2008). After hand polishing to expose the interiors of the grains, we produced backscattered electron and cathodoluminescence images using the JEOL JXA-8900R electron probe microanalyzer at the University of Maryland.

The cores of 49 and 175 zircon grains were dated from samples 09G-35.3 and 09G-37.9, respectively, by laser ablation–inductively coupled plasma–mass spectrometry in the Arizona LaserChron Center at the University of Arizona, taking care to avoid multiple cathodoluminescence zones, inclusions, and cracks. Ablation of the zircon was performed using a New Wave UP193HE Excimer laser and a spot diameter of 30 μm. The ablated zircon was carried in helium into the plasma source of a Nu Plasma HR multi-collector mass spectrometer, and analyses followed the protocols described in Martin et al. (2015).

Corrections for inter-element fractionation of Pb/U and common Pb, as well as other data reduction, were performed off-line using an Excel program developed at the Arizona LaserChron Center. We removed from further consideration analyses with: (1) high ^{204}Pb, (2) greater than 5% error on the $^{206}Pb/^{207}Pb$ date, (3) greater than 5% error on the $^{206}Pb/^{238}U$ date, (4) greater than 25% normal discordance or 8% reverse discordance, (5) high U concentration, or (6) high U/Th ratio. The remaining analyses were used in our interpretations (**Table S1; Fig. 3**). Isoplot was used to calculate weighted means and to produce concordia and probability density plots (Ludwig, 2008).

$^{206}Pb/^{238}U$ dates are usually more precise than $^{206}Pb/^{207}Pb$ dates for zircon younger than about 1.4 Ga, whereas the reverse is true for older grains. However, $^{206}Pb/^{207}Pb$ dates are only minimally affected by recent lead loss, so in most cases they more closely indicate the time of crystallization for zircon older than about 1 Ga. Therefore, during interpretation we used $^{206}Pb/^{238}U$ dates for grains younger than 1 Ga and $^{206}Pb/^{207}Pb$ dates for older zircon grains.

STRATIGRAPHIC AND GEOCHRONOLOGICAL CONSTRAINTS

Carbonates of the Dengying platform are sandwiched between the Ediacaran Doushantuo Formation (ca. 635-551 Ma) (Jiang et al., 2011) and the early Cambrian Kuanchuanpu Formation (Steiner et al., 2004) in the southern Shaanxi region (**Fig. 1**). The Dengying Formation at Gaojiashan is subdivided into three intervals, including the Algal Dolomite, Gaojiashan, and Beiwan members (**Fig. 1C**), which are generally correlated with Hamajing, Shibantan, and Baimatuo members, respectively, in the Yangtze Gorges area (Zhou and Xiao,

2007; Zhu et al., 2007; Duda et al., 2015). Based on the 551 Ma U-Pb zircon depositional age of a volcanic ash at the top of the Miaohe Member, which has historically been correlated with Doushantuo Member IV (Condon et al., 2005), and an estimated 541 Ma age for the Ediacaran-Cambrian boundary (Amthor et al., 2003; Chen et al., 2015), the >650 m thick Dengying Formation represents the last 10 million years of the Ediacaran Period. However, a recent chemostratigraphic study of the Miaohe Member (An et al., 2015) demonstrates that the 551 Ma ash bed lies between the Hamajing and Shibantan members of the Dengying Formation, and is thus not relevant to the biogeochemical anomaly (i.e. Shuram Excursion) preserved in the upper Doushantuo Formation (*cf.* Kaufman, 2005).

At the studied section, the Gaojiashan Member is 55 m in thickness, including a siltstone interval in the lower part, repetitious siltstone-mudstone-limestone facies with cryptalgal crinkly laminations in the middle part, and a coarse sandstone/conglomerate at the top (**Fig. 2**) (Cai et al., 2010). The lower Gaojiashan Member contains the enigmatic fossil *Shaanxilithes ningqiangensis* preserved in siltstone facies (Meyer et al., 2012). The middle Gaojiashan Member contains *Conotubus hemiannulatus* and *Gaojiashania cyclus* preserved in thin, normally graded calcisiltite-siltstone beds interpreted as distal event deposits (Cai et al., 2010), followed by the first appearance of the biomineralized animal *Cloudina* preserved in intraclastic limestones approximately 40 m above the base of the succession (**Fig. 1**). A distinctive horizon with bedded gypsum occurs in the upper part of the Gaojiashan Member (**Figs. 1D, 2F-G**).

RESULTS

Detrital zircon from two closely-spaced siltstone beds at 16.7 m (sample 09G-35.3) and 14.1 m (sample 09G-37.9) above the base of the Gaojiashan member yielded a youngest population of four U-Pb ages ranging from 543 to 550 Ma from sample 09G-37.9, with a weighted mean age of 548 ± 8 Ma (MSWD = 0.11) (**Fig. 3, Table S1)**. This maximum depositional age based on detrital zircon ages is consistent with the 551 Ma age estimate for the Miaohe Member beneath the Gaojiashan equivalent Shibantan Member of the Dengying Formation based on U-Pb zircon age from the bedded ash layer (Amthor et al., 2003; Condon et al., 2005; Chen et al., 2015). However, most of the detrital zircons in this study had ages between 750 and 850 Ma, with a scattering of solitary dates spanning from 1300 to 2700 Ma.

In total 113 limestone and calcareous siltstone samples from the Gaojiashan Member were analyzed for elemental abundances and isotopic compositions (**Figs. 4-5; Tables S2-S4**). Carbonate percentages in the samples are generally high (>90%), except in the lower member where limestones and siltstones are interbedded. The stratigraphic trend of $\delta^{13}C_{carb}$ variations reveals a positive carbon isotope excursion (up to +6‰) in the upper part of the Gaojiashan Member, coinciding with the fossil transition from *Conotubus* to *Cloudina*. Coupled with the positive $\delta^{13}C_{carb}$ event, $\delta^{13}C_{org}$ data reveal a negative excursion (down to –30‰); calculated carbon isotope fractionations ($\Delta\delta^{13}C_{carb\text{-}org}$) show peak values up to +36‰ in this interval. Pyrite S isotope ($\delta^{34}S_{pyrite}$) values measured from bulk acidified residues (assuming pyrite S >> organic S) show a wide range from –30‰ to +30‰ in the Gaojiashan Member, with more negative values in the lower half of the section, and more positive values in the upper half. On the contrary, sulfur isotope compositions of carbonate-associated sulfate ($\delta^{34}S_{CAS}$) remain generally invariant around ca. +40‰ throughout the Gaojiashan Member. Both total sulfur (TS) and total organic carbon (TOC) are relatively low through most of the succession, but are elevated in the cloudinid interval. Mg/Ca ratios show the dominance of limestone in the Gaojiashan Member, with higher Mg/Ca, Mn/Sr and Rb/Sr ratios found only in dolostones interbedded with siltstones in the lower Gaojiashan Member. Sr/Ca ratios reveal a positive excursion in the upper section, mimicking the $\delta^{13}C_{carb}$ anomaly, whereas Ce/Ce* ratios through the section remain constant at values near to 0.5, with the exception of two samples at the top of the Gaojiashan Member with higher values.

DISCUSSION

Diagenesis

Confidence in our ability to interpret environmental changes associated with the paleontological transitions in the Gaojiashan requires that we evaluate the degree of alteration of the limestone samples. Based on the low Mn/Sr and Rb/Sr, and the smooth temporal trends in other geochemical indicators defined by high-resolution sampling, the limestones appear to be especially well preserved (**Fig. 4**). However, insofar as

carbonates are susceptible to isotopic exchange with meteoric or hydrothermal fluids after burial, stable isotope compositions of carbonate phases might reflect diagenetic overprints over depositional signatures. For example, the lithification of marine carbonates associated with the flushing of meteoric fluids could cause coupled depletions in both ^{13}C and ^{18}O, assuming the alkalinity was sourced from soil respiration (Knauth and Kennedy, 2009). Isotopic coupling in carbonates might also result from burial diagenesis (Derry, 2010; Bristow et al., 2011) assuming hot fluid temperatures and alkalinity formed through anaerobic processes. In either case the carbonates would be predictably recrystallized or contain appreciable amounts of neomorphic calcite. These petrographic features are not observed in the fine-grained Gaojiashan limestones, which reveal a significant positive $\delta^{13}C_{carb}$ excursion whereas $\delta^{18}O_{carb}$ values remain steady. A cross plot of the carbon and oxygen isotope abundances in these samples reveals no positive correlation (**Fig. 5, lower panel**). Insofar as oxygen isotopes would be more likely to be altered during water-rock interactions (Jacobsen and Kaufman, 1999), the $\delta^{13}C_{carb}$ excursion recorded in the Gaojiashan Member is likely to reflect true secular changes in seawater composition.

The degree of carbonate preservation may also be evaluated through the analyses of CAS abundances and sulfur isotope compositions. Published studies have shown that CAS in marine carbonates may be affected by secondary processes related to pyrite oxidation (Marenco et al., 2008), which could occur in the outcrop or in the laboratory, or the addition of secondary atmospheric sulfate (SAS) to carbonates exposed in desert environments (Peng et al., 2014). On the other hand, CAS studies of modern carbonate sediments where there was active pore-water sulfate reduction indicate minimal alteration of bulk carbonate sulfur isotope compositions (Lyons et al., 2004). While Gaojiashan CAS abundances are generally low (ranging from near 0 to 150 ppm), their $\delta^{34}S_{CAS}$ values are invariant at ca. +40‰ throughout the succession (**Fig. 5F,G**), suggesting excellent preservation of primary signals (Gill et al., 2008). The sulfur isotope invariance, which is notably consistent with $\delta^{34}S_{sulfate}$ analyses of bedded anhydrites (ca. +40‰) in equivalent terminal Ediacaran strata from Oman (Fike and Grotzinger, 2008), supports the view that the Gaojiashan carbonates are exceptionally well preserved and likely reflective of global seawater conditions.

To further evaluate diagenesis in the Gaojiashan Member samples we compared abundances of TOC and pyrite against each other, as well as with their carbon and sulfur isotope compositions, respectively. In neither case do we see a systematic relationship (**Fig. 5 lower panel**), although the two samples with the highest TOC do have the lowest $\delta^{13}C$ signatures. TOC might change by either microbial (Borowski et al., 1996; Jørgensen et al., 2004; Ries et al., 2009; Borowski et al., 2013) or thermochemical (Cai et al., 2001; Cai et al., 2003; Cai et al., 2004) sulfate reduction after deposition, which could result in progressive ^{34}S-enrichment of product sulfide preserved as pyrite. However, the sedimentary rocks have not been buried deeply enough to drive the thermal reactions. Furthermore, we find no systematic relationship in TOC–TS or TOC–$\delta^{34}S$ cross plots, suggesting that these secondary processes did not significantly impact the Gaojiashan samples.

Redox constraints for the Gaojiashan Member

Multiple lines of evidence suggest that the paleontological transition in the middle Gaojiashan Member is accompanied by strong ocean stratification (**Figs. 5, 6**). Support for this interpretation comes from the negative excursion in the ^{13}C abundance of total organic carbon (TOC) – which mirrors the positive $\delta^{13}C_{carb}$ excursion – resulting in the greatest degree of $\Delta\delta^{13}C$ in the *Cloudina* interval (**Fig. 5 A-C**). In light of the abundance of microbial fabrics in both the Gaojiashan Member (Cai et al., 2010) and the Nama group (Bouougri and Porada, 2007), these decoupled chemostratigraphic carbon isotope trends could plausibly have resulted from organic matter derived from benthic microbial mats where anaerobic chemoautotrophs utilized locally recycled ^{13}C-depleted DIC to form biomass with lower $\delta^{13}C_{org}$ values (Des Marais, 1990; Hayes, 1993; Falkowski et al., 2008; Houghton et al., 2014). Alternatively, there may have been an enhanced flux of organic matter derived from anoxygenic photoautotrophs such as green and purple sulfur bacteria that utilize H_2S as a source of electrons during photosynthesis (Johnston et al., 2009). These photoautotrophs typically exist along redox chemoclines and utilize respired CO_2, which is typically depleted in ^{13}C relative to its atmospheric equivalent (e.g. Brocks et al., 2005). In either case, the spread of anoxic/euxinic conditions across the platform would have promoted organic matter burial (Hayes et al., 1983) and the positive $\delta^{13}C_{carb}$ excursion. High abundances of organic S compounds, indicative of euxinic conditions, are also revealed by biomarker studies

of the Gaojiashan-equivalent Shibantan Member (Duda et al., 2014). Further evidence for the spread of anoxia associated with the decoupled $\delta^{13}C$ excursions is found in the profoundly negative $\delta^{238}U$ signatures of Gaojiashan limestones (Zhang et al., 2015), and our sulfur isotope measurements.

Chemostratigraphic analyses of the Gaojiashan Member reveal a profound rise in $\delta^{34}S_{pyrite}$ values from as low as –30‰ in the lower half of the member to peak values near +30‰ between 35 and 40 m before falling rapidly to values averaging around +10‰ in the *Cloudina*-bearing beds (**Fig. 5G**). In contrast, the $\delta^{34}S$ of carbonate associated sulfate (CAS) remain steady at values of ca. +40‰ throughout the Gaojiashan Member. The calculated sulfur isotope contrasts ($\Delta\delta^{34}S$) range widely in the lower half of the succession, with a maximal value of 72‰, but in the upper half $\Delta\delta^{34}S$ is relatively constant at ca. 30 – 35‰ (**Fig. 5H**). Interpreting the environmental significance of these remarkable stratigraphic variations requires the recognition that the $\delta^{34}S_{CAS}$ and $\delta^{34}S_{pyrite}$ signatures are inherited from different parts of the depositional basin. Sulfate incorporation into primary carbonate sediments would occur within the water column, whereas pyrite would form either in euxinic bottom waters or within sediments. Considering this spatial separation, local sulfate availability could dictate the $\delta^{34}S$ isotopic difference between CAS and pyrite, particularly if pyrite is formed in non-bioturbated and microbially-sealed sediments where the water-sediment interface represents a significant diffusion barrier (Seilacher and Pflüger, 1994; Bottjer et al., 2000; Bouougri and Porada, 2007; Fike et al., 2008; Fike et al., 2009). While such a scenario might apply to discrete intervals within the Gaojiashan – including the *Shaanxilithes* and *Conotubus* zones (**Fig. 5H**) – other parts of the succession have measured $\Delta\delta^{34}S$ differences that are significantly larger. Furthermore, the constancy of the $\delta^{34}S_{CAS}$ values through the Gaojiashan suggests that the perturbation in the terminal Ediacaran sulfur cycle did not involve changes in the marine sulfate isotopic composition. Thus, the ~60‰ shift in $\delta^{34}S$ of pyrite from the lower to the upper Gaojiashan Member may require a change in biologically-induced fractionations involving both the reductive and oxidative paths of the sulfur cycle (i.e. bacterial S disproportionation, or BSD) (Canfield and Thamdrup, 1994), or microbial sulfate reduction (MSR) with very low sulfate reduction rates (SRR) (Canfield et al., 2010; Leavitt et al., 2013; Wu and Farquhar, 2013; Wing and Halevy, 2014).

In the case of BSD, sulfur is recyled via both reductive and oxidative pathways. On the reductive side, the magnitude of kinetic sulfur isotope fractionation (ε_{SR}) has been observed to correlate directly with extracellular sulfate concentrations. Experiments from pure cultures of sulfate reducers indicate maximal fractionation of 66‰ at sulfate concentrations similar to modern seawater at 28 mM (Sim et al., 2011), while ε_{SR} may be suppressed at very low sulfate abundances (<200 μM) (Habicht et al., 2002). On the oxidative side, the sulfide produced through MSR is typically re-oxidized to elemental sulfur, which is subsequently disproportionated to sulfate and sulfide, by coupling with the reduction of O_2, NO_3^-, or iron and manganese compounds (Canfield and Thamdrup, 1994). Disproportionation reactions thus can significantly augment the fractionations induced during MSR, resulting in isotopic contrasts between reactant sulfate and product sulfide of greater than 70‰ (**Fig. 5H**).

Alternatively, very low rates of MSR may also lead to large fractionations. Recent studies of lacustrine euxinic systems indicate that >70‰ fractionations are achievable by both isolated and natural populations of sulfate reducers (Canfield et al., 2010; Gomes and Hurtgen, 2015). Furthermore, environmentally controlled experiments suggest that MSR-related fractionation could be strain specific (Bradley et al., 2016), or related to sulfate reduction rates that are dependent on the availability of organic substrates as electron donors (Canfield et al., 2010; Leavitt et al., 2013; Leavitt, 2014; Wing and Halevy, 2014; Gomes and Hurtgen, 2015). In this case the magnitude of fractionation is inversely correlated with the rate of sulfate reduction (e.g., Xiao et al., 2010). With these constraints in mind, the $\Delta\delta^{34}S$ >70‰ in the lower interval of the Gaojiashan may reflect BSD coupled with MSR, or result solely from MSR with very low SRR. The former scenario is consistent with sulfide oxidation occurring along a chemocline above euxinic deep waters (**Fig. 6A**), which is our preferred interpretation for this marginal marine basin.

Based on systematic studies of modern environments and Phanerozoic shales (Berner and Raiswell, 1983; Berner and Raiswell, 1984), very low C/S ratios might indicate euxinic marine conditions. Although the C/S proxy is not well calibrated for carbonates, the preponderance of Gaojiashan limestones with values <1 (**Fig. 5 lower panel**) suggests the possibility of euxinic conditions in the depositional basin. This view is

consistent with the high Ce/Ce* values in the upper Gaojiashan samples (**Fig. 4H**), although carbonates have notoriously low REE abundances and should thus be interpreted with caution.

Global indicators of dynamic redox conditions

Chemostratigraphic comparison of terminal Ediacaran successions in South China, Oman, and Namibia reveal both similarities and differences, suggesting local overprint of global signals in some basins (e.g., Loyd et al., 2013; Wood et al., 2015) (**Fig. 7**). Global conditions appear to be reflected in the similarity in the magnitude and direction of isotope trends in South China and Oman. For example, in the uppermost Buah Formation of Oman, paired CAS-pyrite measurements reveal large magnitude sulfur isotope fractionations (with maximal $\Delta\delta^{34}S$ ~50‰) prior to the first occurrence of *Cloudina* (Conway Morris et al., 1990), just as we document for the lower Gaojiashan Member. The large fractionation seen in two basins suggests the dominanace of sulfur disproportionation reactions (Fike et al., 2006; Fike and Grotzinger, 2008), which is supported by a recent multiple sulfur isotope study indicating enhanced sulfide re-oxidation in the uppermost Buah (Wu et al., 2015). In this interval disproportionation reactions likely dominated over MSR insofar as the latter would bediscouraged if there was active photoautotrophic sulfide oxidation (**Fig. 6A**) (Habicht and Canfield, 2001). Stratigraphically higher in the Ara Formation where *Cloudina* occurs in carbonates interbedded with evaporites, the $\delta^{34}S$ compositions of pyrite and CAS are notably invariant with a smaller magnitude of fractionation (ca. 30‰) (Fike and Grotzinger, 2008), again exactly matching our observations from the upper Gaojiashan. The ^{34}S enrichments in pyrite and the smaller sulfur isotope differences between reduced and oxidized phases are best explained by high rate of MSR, which we view as the dominant sulfur metabolism associated with the spread of anoxic bottom waters (**Figs. 6B-C**). In sum, the correlated observations from South China and Oman indicate a global environmental control on biological sulfur fractionations.

To the contrary, chemostratigraphic data from *Cloudina*-bearing strata of the Nama Group in southern Namibia provide a completely different pattern of ^{34}S enrichments and fractionation. In this case strongly positive $\delta^{34}S_{pyrite}$ values are most-often paired with anomalously low and scattered $\delta^{34}S_{CAS}$ values, resulting in inversely fractionated $\Delta\delta^{34}S$ values (Ries et al., 2009). Stratigraphically coherent CAS results are only seen in the Omkyk Member where there is a positive $\delta^{34}S_{CAS}$ shift from ca. +10 up to +40‰, which is similar to the trend encompassing the transition to the *Cloudina*-bearing beds in Oman and South China (**Fig. 7**), and in the uppermost Spitzkop Member below the Ediacaran-Cambrian boundary. In this case, however, the CAS sulfur isotope compositions are depleted in ^{34}S by ~ 20‰ relative to equivalent upper Ara strata in Oman. Based on our experience with quantitative preparation techniques, it would appear that the Namibian CAS samples were not adequately leached of non-CAS components. In contrast to our extensive efforts to remove the non-carbonate fraction (see Methods), Ries et al. (2009) leached the CAS powders with Milli-Q water only once, and this is unlikely to have removed sulfate on mineral surfaces formed through pyrite oxidation (Marenco et al., 2008) or secondary atmospheric sulfate (SAS) (Peng et al., 2014). The presence of these contaminants would cause $\delta^{34}S_{CAS}$ values to be more negative and hence would not reflect depositional signatures (Wotte et al., 2012). In our view the inversely fractionated sulfur isotopes from this succession should be interpreted with caution, although they do highlight the potential redox differences between equivalent terminal Ediacaran basins.

In addition, there are notable contrasts in carbon isotope anomalies among the terminal Ediacaran successions in South China, Oman, and Namibia. Chemostratigraphic data from the Dengying Formation suggests the possibility of three separate positive excursions **(Fig. 1)**, with their different stratigraphic expanses likely associated with varying sediment accumulation rates. In contrast, there is significant $\delta^{13}C_{carb}$ variability in the evaporite-rich succession from Oman (Fike and Grotzinger, 2008; Wu et al., 2015), including negative anomalies within the cloudinid interval interspersed with at least two positive excursions **(Fig. 7)**. In Namibia there is only one post-Shuram positive $\delta^{13}C_{carb}$ excursion followed by a long plateau of moderately positive (ca. +1 to +3‰) values leading up to the Ediacaran-Cambrian boundary **(Fig. 7)** (Ries et al., 2009). Other terminal Ediacaran successions, including those in northern India, also reveal significant differences in carbon isotope stratigraphic profiles (Kaufman et al., 2006). Taken together, the inter-basinal variations in carbon and sulfur isotope compositions likely reflect redox differences in the depositional environments of the various basins. If

correct, the Ediacaran experiment in animal life must have been spread across a dynamic environmental landscape, which may help to explain the distribution of geographically unique assemblages (Narbonne et al., 2014)..

Enhanced alkalinity in the terminal Ediacaran ocean

Compared with carbonates in the underlying Doushantuo Formation (e.g., McFadden et al., 2008), the generally lower TOC contents of the Gaojiashan limestones are notable, and may reflect either depositional or early diagenetic processes. For example, pervasive water column or sediment recycling of organic matter may have decreased original organic carbon contents in sediments. In addition, the anaerobic conversion of simple organic compounds to alkalinity could have resulted in the formation of ubiquitous authigenic carbonates (Higgins et al., 2009; Schrag et al., 2013). Driven by iron or sulfate reduction of available organic substrates, the addition of authigenic carbonate to the sediments would, however, have resulted in a negative (rather than a positive) carbon isotope excursion. Alternatively, the generally lower TOC values may reflect significant dilution by abundant carbonate formed from highly alkaline seawater. In this case the source of the alkalinity was more likely to be from terrestrial weathering, as indicated by the significant rise in $^{87}Sr/^{86}Sr$ in the terminal Ediacaran Period (Kaufman et al., 1993; Kaufman et al., 1997; Halverson et al., 2007; Sawaki et al., 2010). The abundance and carbon isotopic composition of river-derived alkalinity in the Ediacaran Period was likely to be high variable, depending on the differential weathering of bedrock lithologies (e.g. carbonates vs. silicates). In the absence of land plants or extensive microbial surfaces, terrestrial sources of alkalinity need not have been significantly depleted in ^{13}C. Elevated seawater alkalinity at this time is consistent with the presence of aragonite crystal fans preserved in the time-equivalent Nama Group in Namibia (Grotzinger, 2000; Grotzinger et al., 2005; Hall et al., 2013), which records a singular Ediacaran positive $\delta^{13}C_{carb}$ excursion (Kaufman et al., 1991; Saylor et al., 1998). Overall high alkalinity is consistent with the dominance of carbonate in terminal Ediacaran successions worldwide, and may explain the extremely high accumulation rate estimated for the Dengying (i.e. >650 m in ~10 million years), as compared with the underlying Doushatuo (i.e. <200 m in ~84 million years) (**Fig. 1**).

Enhanced terminal Ediacaran alkalinity may also be interpreted from our elemental results from the Gaojiashan, as well as inter- and intra-basinal equivalents. In particular the [Sr] and Sr/Ca data measured from the Gaojiashan limestones reveal positive excursions in step with the positive $\delta^{13}C_{carb}$ anomaly (**Fig. 8**). A similar [Sr] excursion coincident with peak $\delta^{13}C$ compositions of carbonates is noted in the Gaojiashan-equivalent Shibantan Member in the Yangtze Gorges area (Sawaki et al., 2010). A rise in [Sr] is also noted in the broadly equivalent Nama Group in southern Namibia (Ries et al., 2009) although this geochemical anomaly post-dates the first appearance of *Cloudina* and the singular positive $\delta^{13}C$ excursion in the thick sedimentary succession. The apparent [Sr] rise in Namibia is potentially complicated by the admixture of siliciclastics within the carbonates by using aqua regia acid, which would attack both carbonate and siliclastic components in the dissolution procedure of Ries et al. (2009). Nonetheless, all sections show positive [Sr] excursion in *Cloudina*-bearing intervals. For the Gaojiashan, the invariantly low Mg/Ca values of samples suggests that dolomitization played no role in the elemental excursion (**Fig. 4**).

Given that the dominant source of Sr in the ocean is from the chemical weathering of the continental crust (Shields, 2007; McArthur et al., 2012), including both silicates and carbonates, enhanced [Sr] and Sr/Ca values supports the view that terrestrial weathering and the delivery of alkalinity through riverine inputs buffered shallow ocean basins to variable degrees in the terminal Ediacaran Period. The weathering of Ca silicate minerals can be simply represented by the overall reaction (Berner, 2004): $CO_2 + CaSiO_3 \rightarrow CaCO_3 + SiO_2$, which over geological time scales sequesters atmospheric CO_2 into carbonate minerals by liberating Ca^{2+} and HCO_3^- ions that are then carried to seawater by rivers. While terrestrial carbonate weathering is not a geological sink for atmospheric CO_2, the resultant flux of alkalinity does effect overall carbonate saturation state (e.g., Kump et al., 1999; Hoffman and Schrag, 2002; Higgins and Schrag, 2003).

Associated with higher alkalinity and higher carbonate saturation, it should be noted that Sr/Ca may also be controlled by precipitation rate. For biogenic carbonates (e.g., coccoliths) the ratio of Sr to Ca has been widely used as a productivity proxy (e.g., Stoll and Schrag, 2001; Stoll and Bains, 2003) insofar as there is a

strong link between Sr/Ca, export production, and calcification rate (Stoll and Schrag, 2001). Similarly, laboratory experiments reveal that rapid precipitation rates induce greater Sr partitioning into abiotic calcite (Lorens, 1981; Tesoriero and Pankow, 1996; Tang et al., 2008; DePaolo, 2011). Thus, the precipitation rate of carbonate in either *Cloudina* or in inorganic micrite may have additionally influenced the Sr/Ca ratios of the Gaojiashan limestones.

Variable partitioning of strontium by aragonite and calcite relative to seawater may also have resulted in the observed variations of Sr/Ca in the Gaojiashan samples. Strontium has a crystal ionic radius larger than that of Ca^{2+} and thus prefers the more open octahedral crystal structure of aragonite over the smaller hexagonal structure of calcite (Wray and Daniels, 1957; Lorens, 1981). Thus on one hand, the enhancement in [Sr] in the Gaojiashan limestones and their equivalents might reflect a secular change from calcite to aragonite-dominated seas (e.g., Stanley and Hardie, 1998), although the short stratigraphic interval represented by the Gaojiashan Member would seem to preclude this possibility. On the other, the [Sr] excursion might result from post-depositional diagenesis, through which Sr was preferentially flushed from specific horizons in the Gaojiashan Member during neomorphic aragonite-to-calcite transformations (Katz et al., 1972). However, given the excellent petrographic and oxygen isotopic preservation of the samples, the absence of dolomitization, and smooth carbon and sulfur isotope trends, we attribute the elevated Sr/Ca ratios in the *Cloudina* interval to 1) elevated Sr flux from the continents to contemporaneous seawater, and/or 2) enhanced precipitation rate in a carbonate over saturated ocean.

Emerging support for weathering-induced high alkalinity in terminal Ediacaran seawater may come from Ca isotope ($\delta^{44}Ca$) measurements of the Gaojiashan equivalent Shibantan Member. In this unit a sharp negative $\delta^{44}Ca$ excursion (down to 0.3‰) has been interpreted to reflect anomalously high seawater Ca concentrations. The Ca isotope system has been used to make inferences regarding the seawater Ca cycle in deep time (DePaolo, 2004; Nielsen et al., 2011), with a special emphasis on perturbations of $\delta^{44}Ca$ during chemical weathering events. Enhanced chemical weathering in the Cenozoic (between 40 and 10 Ma), for example, has been interpreted based on the presence of negative $\delta^{44}Ca$ excursions (De La Rocha and DePaolo, 2000; DePaolo, 2004). Similarly, a Cretaceous negative $\delta^{44}Ca$ excursion believed to be related to enhanced weathering (Blättler et al., 2011)coincides with a positive $\delta^{13}C$ anomaly and an Oceanic Anoxic Event, all of which match our observations of the Gaojiashan.

In concert, the sedimentological and geochemical observations of *Cloudina*-bearing strata in South China and elsewhere suggest that the terminal Ediacaran ocean was highly alkaline. If correct, high concentrations of Ca and alkalinity well may have enabled the earliest example of calcareous biomineralization by animals.

Environmental context of pyritization and biomineralization

Based on our chemostratigraphic observations of the Gaojiashan Member, the first appearance of *Cloudina* coincided with the development of anoxic and episodically euxinic conditions across the shelf environment. It is likely, however, that this first biomineralized metazoan lived in the oxidized shallower water column and was swept into deeper anoxic settings by storm events (Cai et al., 2010) (**Fig. 5B**). In contrast, our geochemical results suggest that *Conotubus* and other soft-bodied Ediacara biotas thrived at a time of more generally oxidizing conditions within the water column prior to the peak of the $\delta^{13}C$ excursion. In the equivalent Shibantan Member in the Yangtze Gorges region, the soft-bodied organisms are preserved in subtidal environments and are closely associated with abundant bilaterian burrows, suggesting moderate levels of bioturbation (Chen et al., 2013; Chen et al., 2014a; Meyer et al., 2014). It is notable that *Conotubus* and many Ediacara remains, as well as the microbial surfaces, were preserved in these environments through pyritization (Gehling, 1999; Schiffbauer et al., 2014). In the "death mask" model, pyritization of a decomposing metazoan would stabilize its surface and allow the external form of the organism to be imprinted with exquisite detail; in the case of the Gaojiashan Member, similar pyritization process may have also molded *Conotubus* tubes from inside. Based on *in-situ* SIMS $\delta^{34}S$ analyses, it has been proposed that pyritization of *Conotubus* was fueled by the degradation of labile organic tissues through MSR (Schiffbauer et al., 2014) near the sediment-water interface. Consistent with pyritization as a widespread fossilization pathway, many soft-

bodied fossils and associated microbial surfaces in the Gaojiashan and Shibantan exposures are coated with iron oxides and jarosite (an iron-bearing sulfate mineral) that are the oxidative weathering products of early diagenetic pyrite (Hall et al., 2013).

The balance between the ecological pressures and physiological responses that resulted in the biomineralization of *Cloudina* are nicely viewed from the Gaojiashan Member and its equivalents in South China. On one hand, Hua et al. (2003) highlighted the large number of drill holes on *Cloudina* shells in the Dengying Formation and hypothesized that predation tipped the balance towards calcification as a means of protection. On the other, our results emphasize clear temporal changes in seawater chemistry that are associated with this evolutionary milestone. We interpret the geochemical trends to reflect enhanced terminal Ediacaran chemical weathering that introduced nutrients, which drove primary productivity, the spread of anoxia, and higher rates of organic carbon burial. Chemical weathering would also have delivered alkalinity and cations including calcium to seawater, promoting rapid carbonate accumulation in shallow marine settings. In addition, sulfate delivery would have further stimulated MSR, which would provide an additional source of seawater alkalinity depending on the extent of water column anoxia. Biomineralization could then have been a means to remove excess calcium from the newly-developed circulatory systems of evolving metazoans (Simkiss, 1977) in the context of higher overall seawater alkalinity in the terminal Ediacaran Period (Grotzinger et al., 2005).

Studies of Phanerozoic biomineralization further highlight the effect of seawater chemistry on calcification. Although the secretion of biominerals often occurs in internal environments isolated from seawater (Weiner and Dove, 2003), seawater chemistry could indirectly determine skeletal mineralogy by affecting the physiological costs of biomineralization (Knoll, 2003a), thus resulting in distinct patterns of skeleton evolution through Earth history. Indeed, extensive compilation of non-skeletal carbonates and hypercalcifying animals in the Phanerozoic reveals that the Mg/Ca and [Ca] of seawater during periods of aragonite or calcite-dominated seas had a strong influence on skeletal mineralogy (Stanley and Hardie, 1998; Stanley, 2006; Porter, 2010). High-Mg calcite and aragonite shells appear to have dominated under aragonite seas, while shells composed of low-Mg calcite dominated under calcite seas. This pattern is also seen in the Cambrian Period when the first massive biodiversification of skeletal animals occured (Porter, 2007). In the terminal Ediacaran, the widespread appearance of seafloor aragonite fans (Grotzinger, 2000; Grotzinger et al., 2005; Hall et al., 2013) and rapid accumulation of carbonates supports the aragonite sea hypothesis, and is consistent with the inferred high-Mg calcite mineralogy of *Cloudina* (Grant, 1990; Zhuravlev et al., 2012).

Temporal growth in the oceanic sulfate reservoir

Projected to the world stage and viewed through the long lens of Earth history, paired sulfur isotope data in the terminal Ediacaran Gaojiashan Member stand out among the highest $\delta^{34}S_{sulfate}$ values (up to +40‰) and largest S isotope fractionations (ca. +70‰) for the whole Precambrian (**Fig. 7**). This pattern may reflect a strongly stratified ocean (e.g., Jiang et al., 2007; Shen et al., 2008; Li et al., 2010; Shen et al., 2010; Shen et al., 2011), which would be particularly meaningful during the terminal Ediacaran when a putative atmospheric and oceanic oxygenation event occurred (i.e. Neoproterozoic Oxygenation Event, or NOE) (Kaufman et al., 2007; Shields-Zhou and Och, 2011; Och and Shields-Zhou, 2012; Lyons et al., 2014; Liu et al., 2016).

Growth of the Ediacaran sulfate pool has been hypothesized to be associated with the NOE (Fike et al., 2006), which occurred in the aftermath of the Marinoan ice age (ca. 635 Ma). A recent quantative model analysis based on sulfur isotope trends through the Ediacaran Period suggests that oceanic [SO_4^{2-}] was low (<5 mM) in the aftermath of the Marinoan glaciation, but then rose (>5 mM) across the Ediacaran-Cambrian boundary (Algeo et al., 2015). The inflection of sulfate concentrations may well have coincided with the middle Ediacaran Shuram Excursion, a profound negative carbon isotope anomaly (Grotzinger et al., 2011) recognized in multiple sections across the globe including Shuram Formation in Oman and the upper Doushantuo Formation of South China (Cui et al., 2015). Sulfur isotope profiles in both regions reveal a parallel decrease in both $\delta^{34}S_{pyrite}$ and $\delta^{34}S_{CAS}$ (Cui et al., 2015) that likely reflect the significant growth of the Ediacaran sulfate pool (Fike et al., 2006; Halverson and Hurtgen, 2007; Kaufman et al., 2007; McFadden et al., 2008). Consistent with this view, psuedomorphs of gypsum are found in the Shuram equivalent Wonoka

Formation in South Australia (Calver, 2000) and in the Doushantuo (Lu et al., 2013). Above the Shuram, an increasing number of bedded evaporite horizons have been discovered in terminal Ediacaran successions, including the Dengying (Siegmund and Erdtmann, 1994; Duda et al., 2015; and this study) and Ara formations (Fike and Grotzinger, 2010), as well as the Hanseran Evaporite Group in northwestern India (Strauss et al., 2001; Mazumdar and Strauss, 2006).

The trigger for the terminal Ediacaran rise in seawater sulfate remains a question of considerable debate. It has been proposed by Canfield and Farquhar (2009) that the emergence of bioturbation near the Ediacaran-Cambrian boundary was the proximate cause insofar as sediment mixing would result in enhanced sulfide oxidation and recycling (Bottjer et al., 2000; Meysman et al., 2006; Rogov et al., 2012; Chen et al., 2014b). While bioturbation clearly modified ecosystems in the Fortunian Stage of the Cambrian Period (Bottjer et al., 2000; Meysman et al., 2006), there is little support for deep penetration by animals into sedimentary layers dominated by microbial mats in the Shuram or terminal Ediacaran intervals (e.g. Carbone and Narbonne, 2014; Meyer et al., 2014). Moreover, recent investigations have demonstrated that the mixing of sediments on marine shelves remained limited until at least the late Silurian, 120 million years after the Precambrian–Cambrian transition (Tarhan and Droser, 2014; Gingras and Konhauser, 2015; Tarhan et al., 2015).

Alternatively, it is likely that the increase in Ediacaran sulfate concentrations was driven by enhanced oxidative weathering of pyrite in continental and oceanic sediments exposed by sea level regression (Kaufman et al., 2007; Wang et al., 2016). This scenario is consistent with the profound increase in seawater $^{87}Sr/^{86}Sr$ (from ca. 0.7080 to 0.7090) recorded globally in carbonates deposited during the Shuram Excursion (Burns et al., 1994; Calver, 2000; Melezhik et al., 2009; Sawaki et al., 2010; Cui et al., 2015). The Sr isotope shift most likely accompanied enhanced silicate weathering (Kaufman et al., 1993; Halverson et al., 2007; Cui et al., 2015), which led to an increase in the delivery of nutrient and sulfate to the oceans. By stimulating photosynthesis, these continental fluxes would on the one hand result in the oxidation of surface environments, while on the other, the remineralization of organic matter along marginal marine settings would simultaneously resulted in the expansion of oxygen minimum zones (OMZs). Oceanic redox stratification would have simultaneously stimulated the oxidative side of the sulfur cycle through widespread sulfur disproportionation along chemoclines (Canfield and Thamdrup, 1994; Fike et al., 2006; Wu et al., 2015) and the reductive side through microbial sulfate reduction within the anoxic plumes. Both microbial processes would have delivered ^{32}S sulfur as pyrite into the sediments and thereby drove oceanic sulfate compositions to positive $\delta^{34}S$ extremes (Canfield, 2004).

CONCLUSIONS

Terminal Ediacaran strata of the Gaojiashan Member preserve a record of dynamic exogenic carbon and sulfur cycling ultimately driven by tectonic forces, a rise in atmospheric oxygen, and enhanced chemical weathering of the exposed continents. Data from South China suggest that the attendant flux of nutrients and alkalinity increased oceanic productivity and carbonate saturation state, resulting in a redox stratified ocean basin where animals evolved to form calcareous shells, through the combined ecological pressure of predation and the environmental pressure of high carbonate saturation, for the first time in Earth history.

ACKNOWLEDGEMENT

We thank Rebecca Plummer, Mike Evans and Brittney Gaeta for their assistance in the UMD Paleoclimate CoLaboratory. This research is funded by the NASA Exobiology grant (NNX12AR91G to AJK and NNX15AL27G to SX), the NSF Sedimentary Geology and Paleontology grant (EAR0844270 and EAR1528553 to AJK; EAR1528553 to SX), the NSF grant (EAR1032156) to the Arizona LaserChron Center, the AAPG Grants-In-Aid Program Marilyn Atwater Memorial Grant to HC, the Explorers Club Washington Group grant to HC, the Carnegie Institution of Washington Postdoctoral Fellowship to XML, and the National Natural Science Foundation of China grant (41572012) to YC. Thanks to the party chief of the Gaojiashan village Fazhi Li for his warm-hearted assistance in the field. Thanks to James Farquhar and Heather M. Stoll for helpful comments. The manuscript also benefits from constructive reviews by Pedro J. Marenco, Marc

Laflamme and another anomymous reviewer. Thanks to the editor Kurt Konhauser for handling this manuscript.

SUPPORTING INFORMATION

Table S1: U-Pb geochronologic analyses of two detrital zircon samples in the lower Gaojiashan Member.
Table S2: Chemostratigraphic data of carbonate C isotopes of the Doushantuo and Dengying formations plotted in Figure 1.
Table S3: Chemostratigraphic data of C, O, and S isotopes of the Gaojiashan Member.
Table S4: Chemostratigraphic data of major and trace element concentrations of the Gaojiashan Member.

FIGURES CAPTIONS

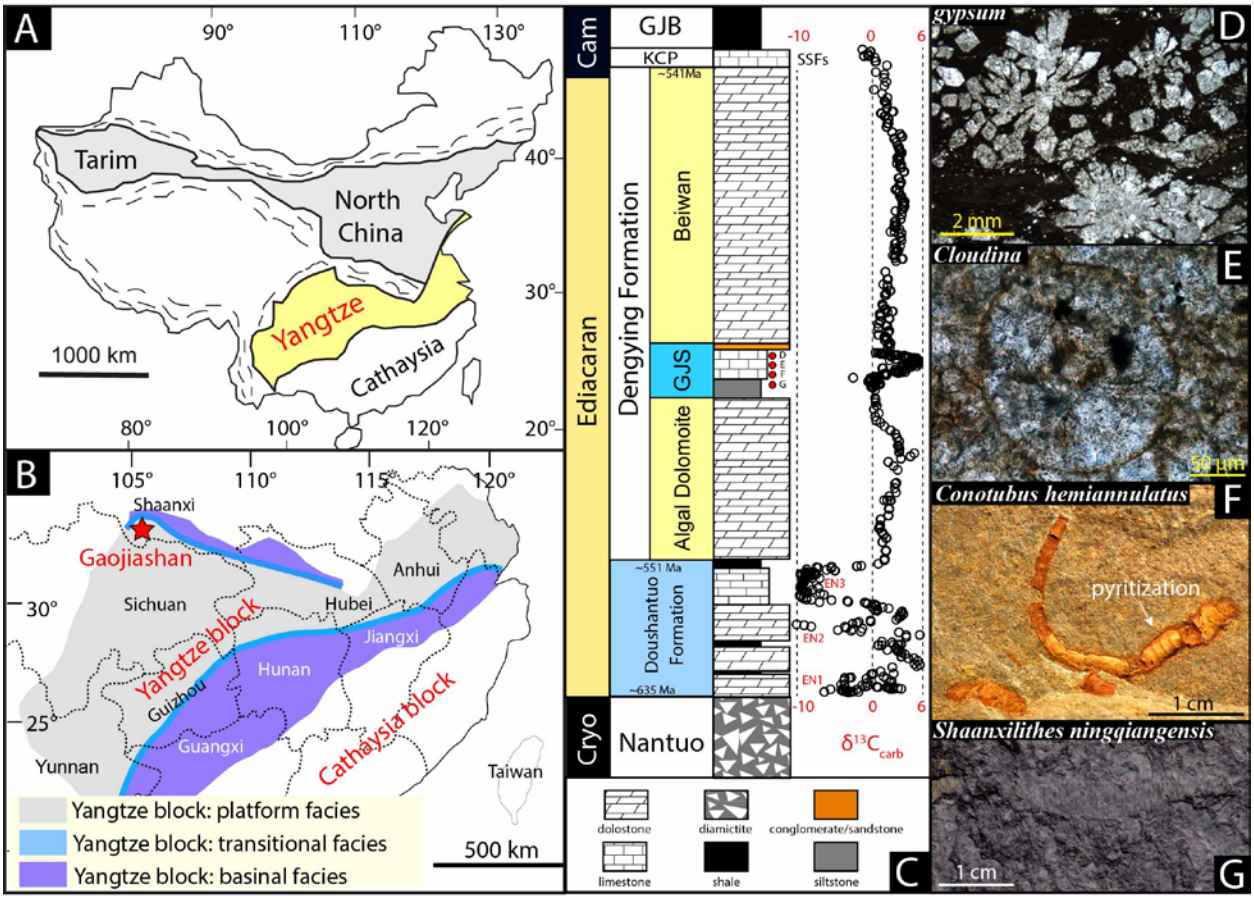

Figure 1. (**A**) Tectonic framework of China, with the Yangtze Craton highlighted in yellow. (**B**) Ediacaran depositional environments on the Yangtze Craton (Jiang et al., 2011). (**C**) $\delta^{13}C_{carb}$ record of the Dengying Formation in the Gaojiashan section. GJS = Gaojiashan, KCP = Kuanchuanpu, GJB = Guojiaba; $\delta^{13}C_{carb}$ data for Doushantuo Formation are from McFadden et al. (2008). (**D**) Calcite pseudomorph after gypsum ca. 46.5 m above the base of the Gaojiashan Member. (**E**) *Cloudina* in the Gaojiashan Member ca. 42 m above the base. (**F**) Pyritized tubular fossil *Conotubus hemiannulatus* (Cai et al., 2011). (G) Enigmatic body fossil *Shaanxilithes ningqiangensis* (Meyer et al., 2012).

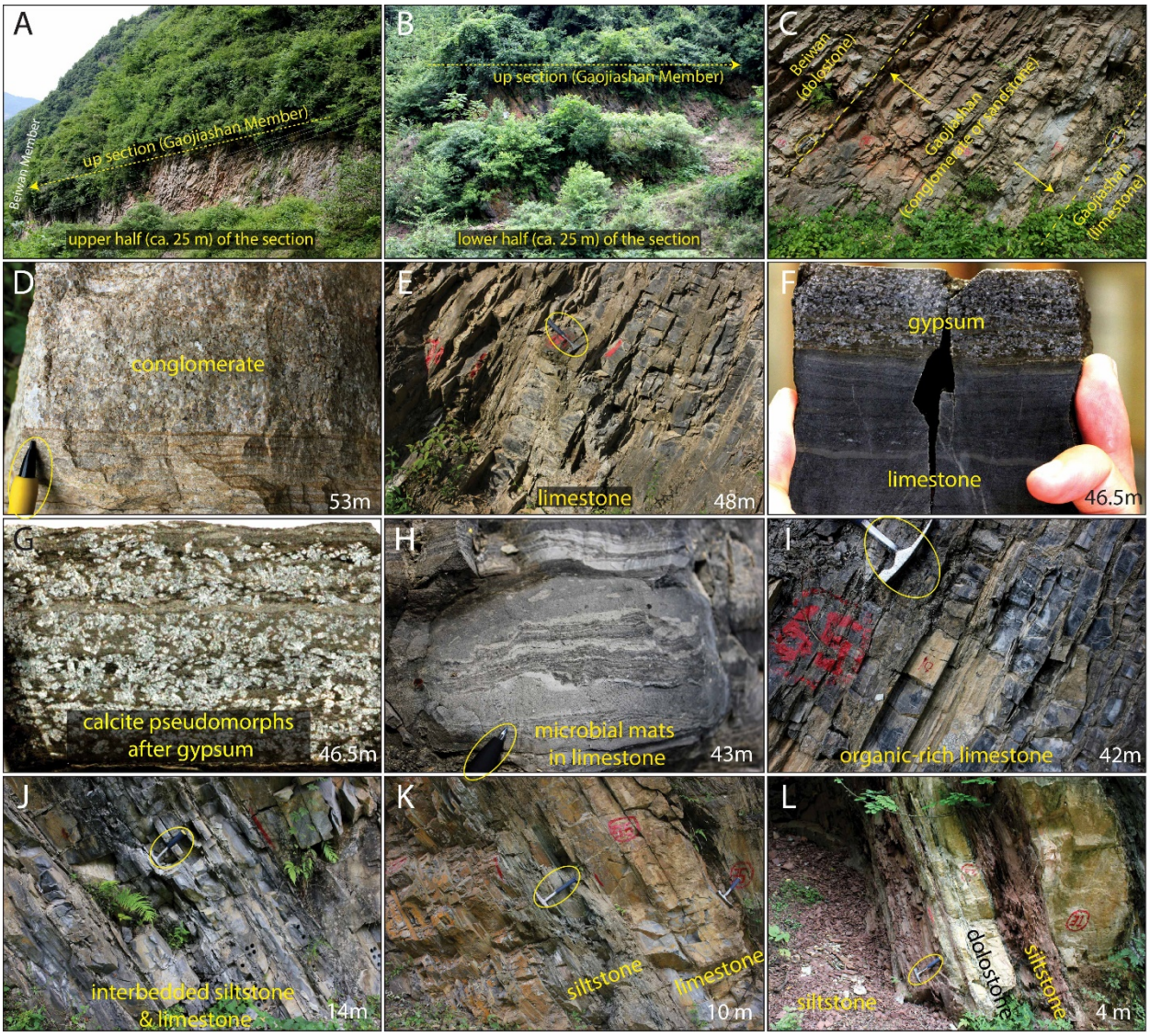

Figure 2: Field photographs of the Gaojiashan Member. Hammers or pencils for scale and meterages above the base of the unit. (**A, B**) An overview of the upper and lower section (each ca. 25 meters in thickness). (**C**) Boundary bewteen the Beiwan and Gaojiashan members. (**D**) Conglomerate in the uppemost interval. (**E**) Bedded limestone at 48 m. (**F, G**) Gypsum pseudomorphs at 46.5 m where crystals have been dissolved and replaced by calcite. (**H, I**) Organic-rich limestones with abudant microbial mats corresponding to the peak of the carbon isotope excursion at ca. 43 m. (**J**) Interbedded siltstone and limestone at 14 m. (**K, L**) Siltstones in the lower Gaojiashan Member.

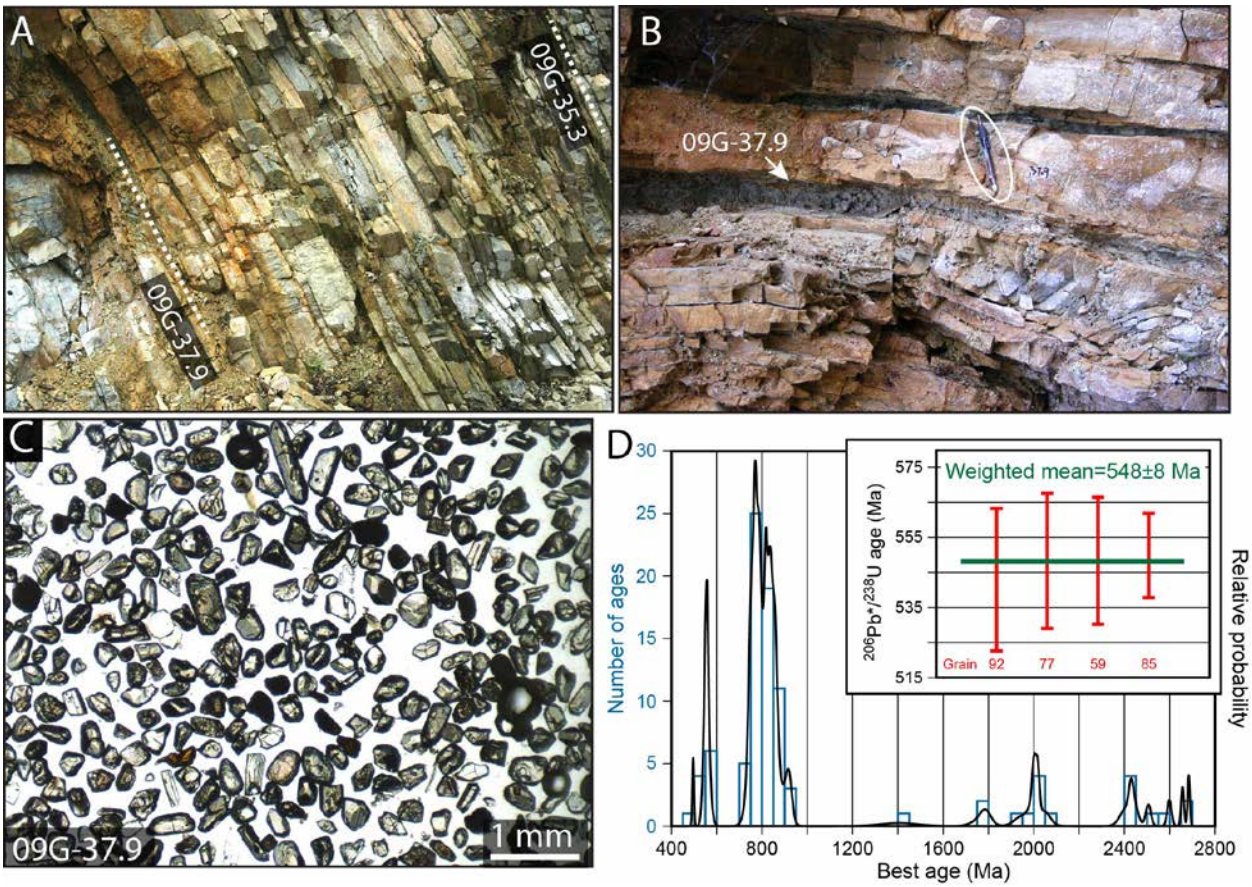

Figure 3: (**A**) Field photo showing the position of the two detrital zircon samples (09G-35.3, 09G-37.9) in the lower Gaojiashan Member. The view is about 3 m wide. (**B**) Close view of bed 09G-37.9. (**C**) Separated and mounted detrital zircon from sample 09G-37.9. (**D**) Histogram and relative probability plot for detrital zircon ages from sample 09G-37.9. Best age is $^{206}Pb/^{238}U$ date for grains younger than 1 Ga and $^{206}Pb/^{207}Pb$ date for older zircon. Histogram bars represent 50 Ma intervals. Inset: $^{206}Pb/^{238}U$ ages for the four youngest analyses with uncertainties that overlap at the 1-sigma level. The weighted mean of these four ages is 548±8 Ma (MSWD=0.11) from which we interpret a maximum possible depositional age of 560 Ma.

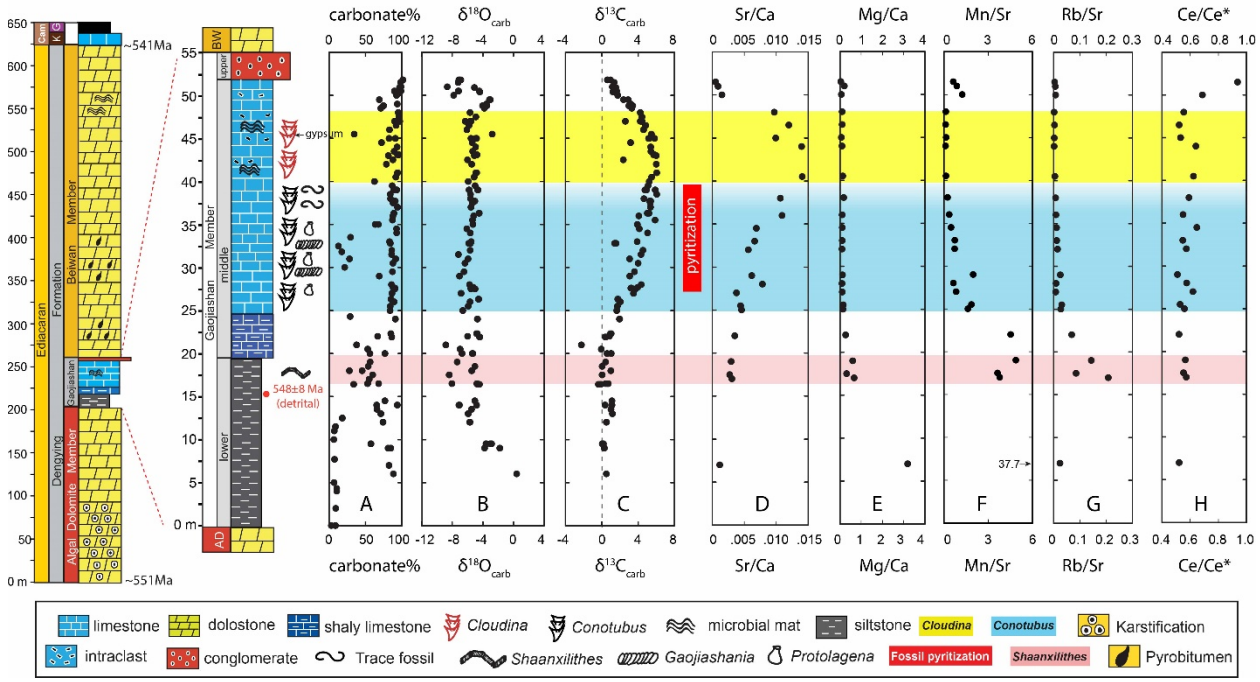

Figure 4: Integrated litho-, bio-, and chemo-stratigraphy of the Gaojiashan Member, including fossil occurrences of *Conotubus* and *Cloudina*, as well as geochemical profiles of carbonate content (wt. %), carbonate carbon ($\delta^{13}C_{carb}$, ‰ V-PDB) and oxygen ($\delta^{18}O_{carb}$, ‰ V-PDB) isotopes, Sr/Ca, Mg/Ca, Rb/Sr, Mn/Sr, and Ce anomaly (Ce/Ce*) calculated using the formula $Ce/Ce^* = Ce_{PAAS}/([Pr]^2_{PAAS}/[Nd]_{PAAS})$ (Ling et al., 2013). K = Kuanchuanpu, G = Guojiaba, Cam = Cambrian, BW = Beiwan, AD = Algal Dolomite.

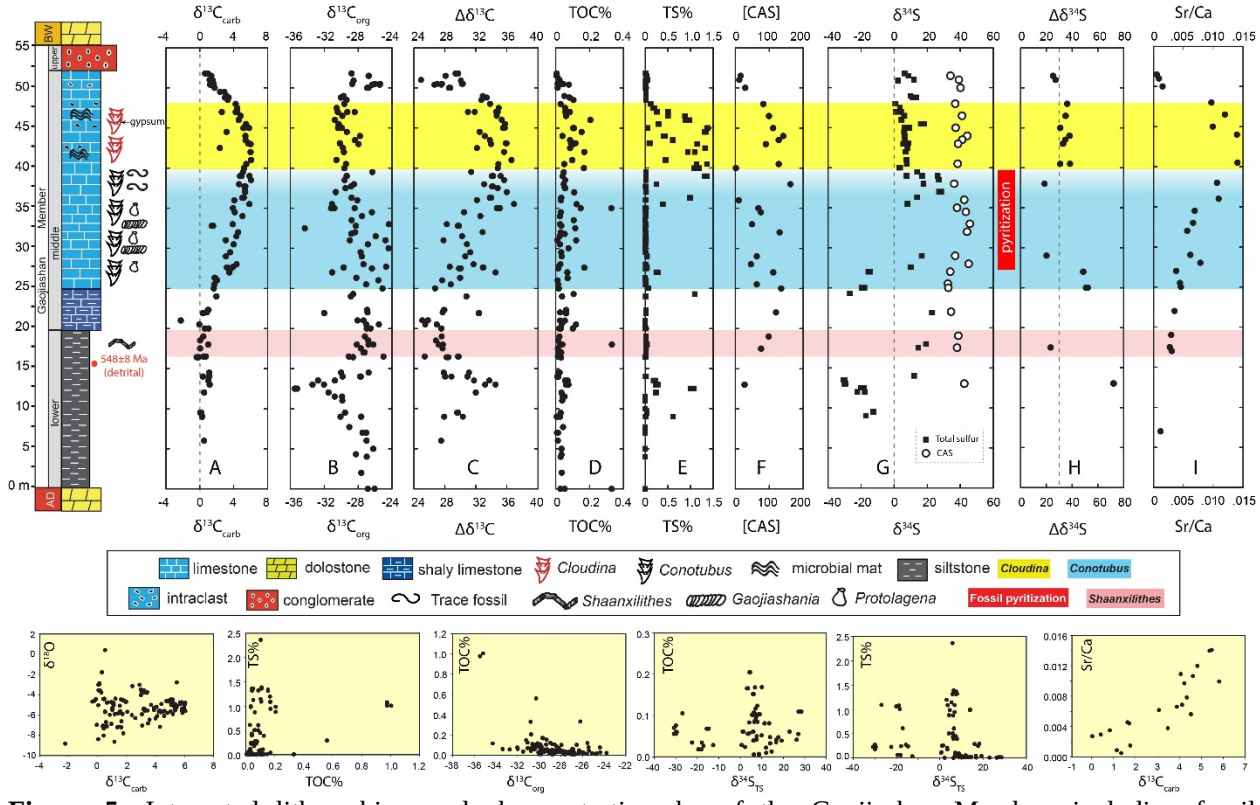

Figure 5: Integrated litho-, bio-, and chemo-stratigraphy of the Gaojiashan Member, including fossil occurrences of *Conotubus* and *Cloudina*, as well as geochemical profiles of carbonate carbon ($\delta^{13}C_{carb}$, ‰ V-

PDB) and organic carbon ($\delta^{13}C_{org}$, ‰ V-PDB) isotopes, carbon isotope fractionations ($\Delta\delta^{13}C_{carb\text{-}org}$), pyrite sulfur ($\delta^{34}S_{TS}$, ‰ V- CDT) and CAS sulfur ($\delta^{13}C_{CAS}$, ‰ V-CDT) isotopes, sulfur isotope fracionations ($\Delta\delta^{34}S_{CAS\text{-}pyrite}$), total organic carbon content (TOC), total sulfur content (TS, dominated by pyrite with trace amount of organic S), carbonate-associated sulfate concentration ([CAS] in ppm). The small panels in the bottom are cross plots of $\delta^{13}C_{carb}$–$\delta^{18}O_{carb}$, TOC–TS, $\delta^{13}C_{org}$–TOC, $\delta^{34}S_{TS}$–TOC , $\delta^{34}S_{TS}$–TS , $\delta^{13}C_{carb}$–Sr/Ca. BW = Beiwan, AD = Algal Dolomite.

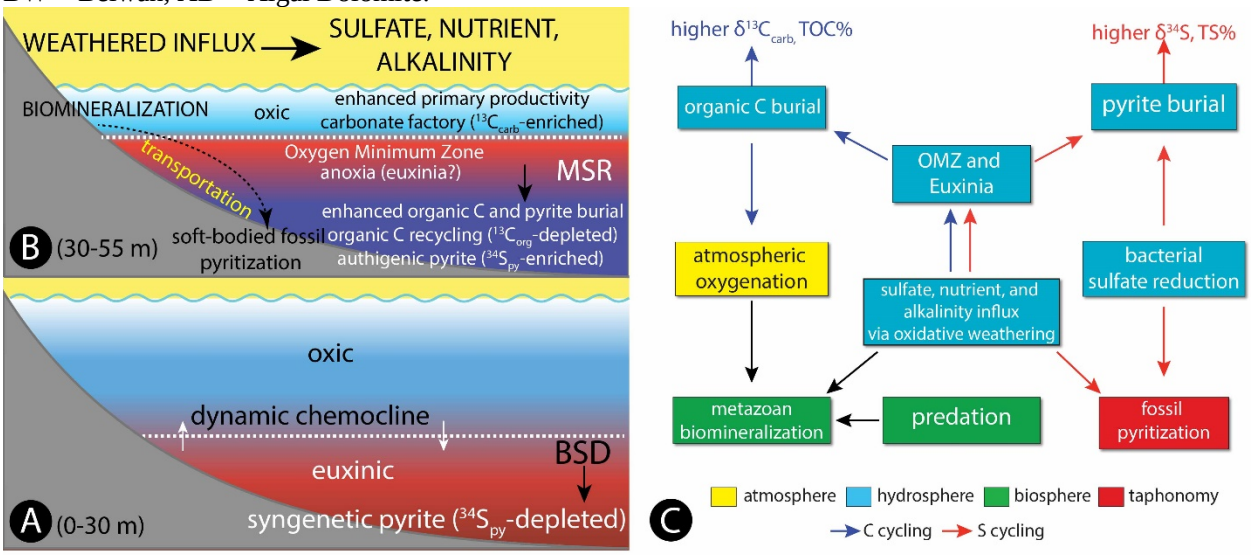

Figure 6. Conceptual weathering and biogeochemical model for the Gaojiashan Member. (**A**) During Stage 1 the basin was stratified with oxic surface water above euxinic deep water. Bacterial S disproportionation (BSD) may be an important contributor to the sulfur cycle. (**B**) During Stage 2 the basin was strongly influenced by the spread of an oxygen minimum zone (OMZ) beneath oxic surface waters. This likely occurred as a result of sea level regression and enhanced continental weathering, which resulted in a larger sulfate pool in the ocean, elevated ocean alkalinity, and microbial sulfate reduction (MSR) as the dominant pathway for microbioal sulfur cycling. (**C**) Biogeochemical feedback that link the carbon and sulfur cycles to atmospheric oxygenation, animal evolution, and fossil preservation.

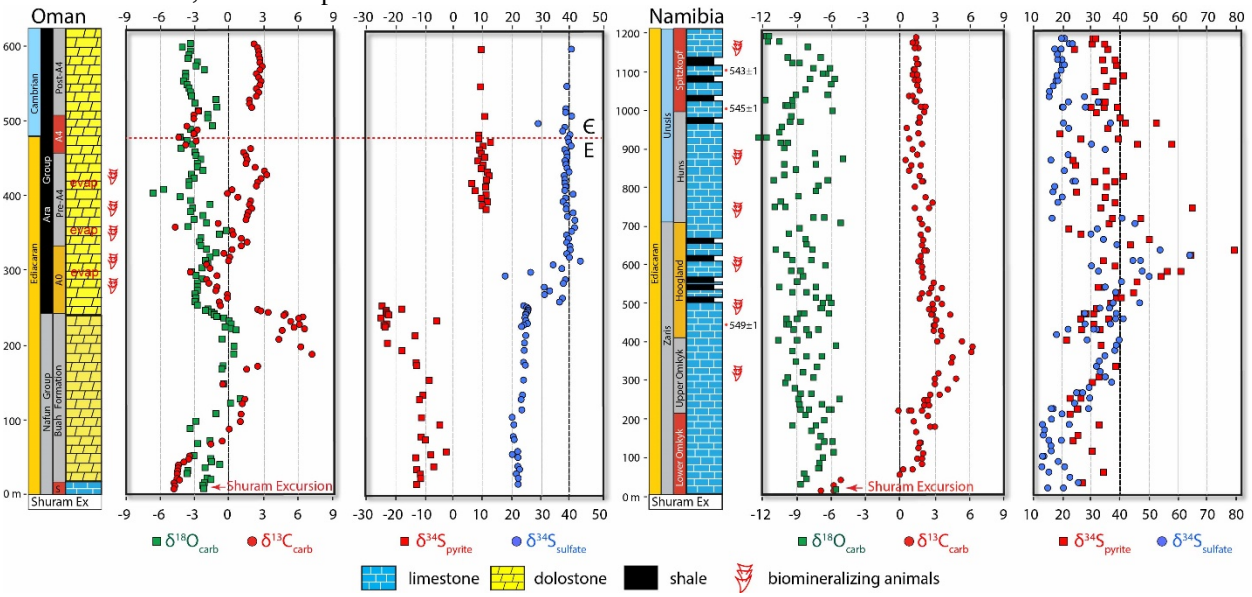

Figure 7: Integrated carbon and sulfur isotopic profiles from late Ediacaran strata in Oman (Fike and Grotzinger, 2008) and Namibia (Ries et al., 2009). The remarkable difference in sulfur isotope trends between Oman and Namibia may result from effects of local conditions (e.g. different organic carbon flux, sulfate

concentration) on microbial sulfate reduction rate and sulfur isotope fractionations, but may also reflect analytical issues (see text).

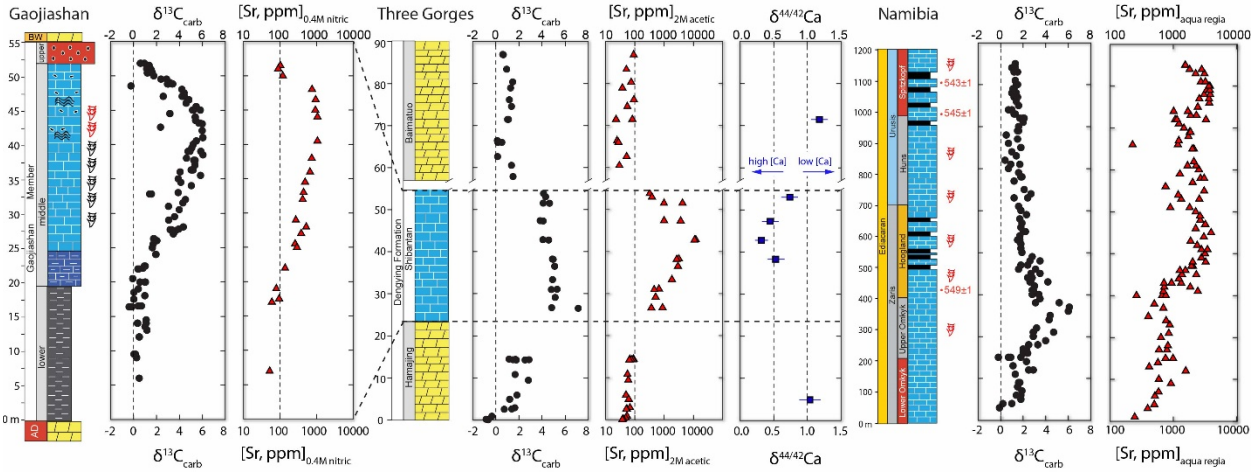

Figure 8. Integrated litho-, bio-, and chemo-stratigraphy of the terminal Ediacaran Gaojiashan Member in the study area, Yangtze Gorges area, and Namabia, including geochenical profiles of carbonate carbon isotopes ($\delta^{13}C_{carb}$, ‰ V-PDB), strontium concentration ([Sr] in ppm, plotted in log scale), and $\delta^{44/42}Ca$ (‰). Data for the section in Yangtze Gorges area are from Sawaki et al. (2010) and Sawaki et al. (2014). Data for the section in Namibia are from Ries et al. (2009). Note that the Sr concentrations are measured by using different acids in different studies. The negative $\delta^{44}Ca$ excursion in the Gaojiashan-equivalent Shibantan Member has been interpreted to reflect high Ca concentration in terminal Ediacaran seawater (Sawaki et al., 2014).

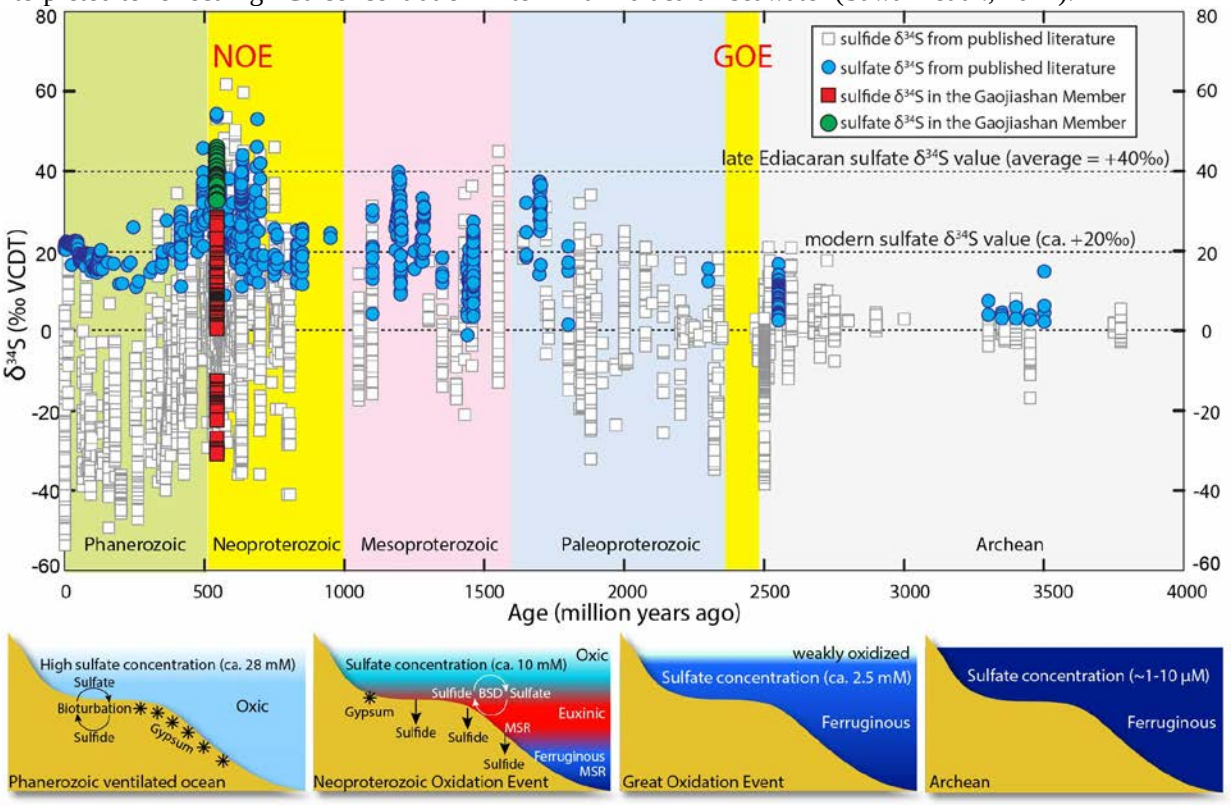

Figure 9. Evaporite, CAS, and pyrite sulfur isotope data through Earth history. Paired $\delta^{34}S$ data are compiled from the literature [after (Canfield and Farquhar, 2009; Och and Shields-Zhou, 2012; Sahoo et al., 2012)]. Recently published Neoarchean $\delta^{34}S$ data have also been included (e.g. Paris et al., 2014; Zhelezinskaia et al., 2014). The sulfate concentration constraints are ca. 1-10 μM during Archean (Habicht et al., 2002; Zhelezinskaia et al., 2014), ca. 2.5 mM after the GOE (Shen et al., 2002; Canfield, 2004; Kah et al., 2004;

Hurtgen et al., 2005; Bekker et al., 2006; Canfield and Farquhar, 2009; Reuschel et al., 2012), and ca. 10 mM during NOE (Canfield and Farquhar, 2009; Algeo et al., 2015). $\delta^{34}S_{sulfate}$ compostion of the terminal Ediacaran ocean (ca. +40‰) was determined by measurements of bedded evaporites in Oman (Fike and Grotzinger, 2008). GOE = Great Oxidation Event; NOE = Neoproterozoic Oxidation Event. The four conceptual biogeochemical models for redox architectures of the ocean during Archean, GOE, NOE and Phanerozoic are shown in the panels beneath the time-series data. See the main text for detailed discussions.

REFERENCES

Algeo, T.J., Luo, G.M., Song, H.Y., Lyons, T.W., Canfield, D.E., 2015. Reconstruction of secular variation in seawater sulfate concentrations. Biogeosciences, 12(7): 2131-2151, doi:10.5194/bg-12-2131-2015

Amthor, J.E., Grotzinger, J.P., Schröder, S., Bowring, S.A., Ramezani, J., Martin, M.W., Matter, A., 2003. Extinction of Cloudina and Namacalathus at the Precambrian-Cambrian boundary in Oman. Geology, 31(5): 431-434, doi:10.1130/0091-7613(2003)031<0431:eocana>2.0.co;2

Bekker, A., Karhu, J., Kaufman, A., 2006. Carbon isotope record for the onset of the Lomagundi carbon isotope excursion in the Great Lakes area, North America. Precambrian Research, 148(1): 145-180, doi:10.1016/j.precamres.2006.03.008

Bengtson, S., Zhao, Y., 1992. Predatorial borings in late Precambrian mineralized exoskeletons. Science, 257(5068): 367-369

Berner, R.A., 2004. The Phanerozoic carbon cycle: CO_2 and O_2. Oxford University Press, New York.

Berner, R.A., Raiswell, R., 1983. Burial of organic carbon and pyrite sulfur in sediments over Phanerozoic time: a new theory. Geochem. Cosmochim. Acta, 47: 855-862, doi:10.1016/0016-7037(83)90151-5

Berner, R.A., Raiswell, R., 1984. C/S method for distinguishing freshwater from marine sedimentary rocks. Geology, 12(6): 365-368, doi:10.1130/0091-7613(1984)12<365:CMFDFF>2.0.CO;2

Blättler, C.L., Jenkyns, H.C., Reynard, L.M., Henderson, G.M., 2011. Significant increases in global weathering during Oceanic Anoxic Events 1a and 2 indicated by calcium isotopes. Earth and Planetary Science Letters, 309(1): 77-88, doi:10.1016/j.epsl.2011.06.029

Borowski, W.S., Paull, C.K., Ussler, W., 1996. Marine pore-water sulfate profiles indicate in situ methane flux from underlying gas hydrate. Geology, 24(7): 655-658

Borowski, W.S., Rodriguez, N.M., Paull, C.K., Ussler, W., 2013. Are ^{34}S-enriched authigenic sulfide minerals a proxy for elevated methane flux and gas hydrates in the geologic record? Marine and Petroleum Geology, 43: 381-395, doi:10.1016/j.marpetgeo.2012.12.009

Bottjer, D.J., Hagadorn, J.W., Dornbos, S.Q., 2000. The Cambrian substrate revolution. GSA today, 10(9): 1-7

Bouougri, E., Porada, H., 2007. Mat-related features from the Terminal Ediacaran Nudaus Formation, Nama Group, Namibia. In: Schieber, J., Bose, P.K., Eriksson, P.G., Banerjee, S., Sarkar, S., Altermann, W., Catuneanu, O. (Eds.), Atlas of Microbial Mat Features Preserved within the Siliciclastic Rock Record. Elsevier, pp. 214-221

Bradley, A.S., Leavitt, W.D., Schmidt, M., Knoll, A.H., Girguis, P.R., Johnston, D.T., 2016. Patterns of sulfur isotope fractionation during microbial sulfate reduction. Geobiology, 14: 91-101, doi:10.1111/gbi.12149

Brennan, S.T., Lowenstein, T.K., Horita, J., 2004. Seawater chemistry and the advent of biocalcification. Geology, 32(6): 473-476, doi:10.1130/g20251.1

Bristow, T.F., Bonifacie, M., Derkowski, A., Eiler, J.M., Grotzinger, J.P., 2011. A hydrothermal origin for isotopically anomalous cap dolostone cements from south China. Nature, 474(7349): 68-71, doi:10.1038/nature10096

Brocks, J.J., Love, G.D., Summons, R.E., Knoll, A.H., Logan, G.A., Bowden, S.A., 2005. Biomarker evidence for green and purple sulphur bacteria in a stratified Palaeoproterozoic sea. Nature, 437(7060): 866-870

Burns, S.J., Haudenschild, U., Matter, A., 1994. The strontium isotopic composition of carbonates from the late Precambrian (~560-540 Ma) Huqf Group of Oman. Chemical Geology, 111(1–4): 269-282, doi:10.1016/0009-2541(94)90094-9

Butterfield, N., 2009. Oxygen, animals and oceanic ventilation: an alternative view. Geobiology, 7(1): 1-7, doi:10.1111/j.1472-4669.2009.00188.x

Butterfield, N.J., 2011. Animals and the invention of the Phanerozoic Earth system. Trends in Ecology & Evolution, 26(2): 81-87, doi:10.1016/j.tree.2010.11.012

715 Cai, C., Hu, W., Worden, R.H., 2001. Thermochemical sulphate reduction in Cambro–Ordovician carbonates
716 in Central Tarim. Marine and Petroleum Geology, 18(6): 729-741, doi:10.1016/S0264-
717 8172(01)00028-9
718 Cai, C., Worden, R.H., Bottrell, S.H., Wang, L., Yang, C., 2003. Thermochemical sulphate reduction and the
719 generation of hydrogen sulphide and thiols (mercaptans) in Triassic carbonate reservoirs from the
720 Sichuan Basin, China. Chemical Geology, 202(1): 39-57, doi:10.1016/S0009-2541(03)00209-2
721 Cai, C., Xie, Z., Worden, R.H., Hu, G., Wang, L., He, H., 2004. Methane-dominated thermochemical sulphate
722 reduction in the Triassic Feixianguan Formation East Sichuan Basin, China: towards prediction of
723 fatal H 2 S concentrations. Marine and Petroleum Geology, 21(10): 1265-1279,
724 doi:10.1016/j.marpetgeo.2004.09.003
725 Cai, Y., Hua, H., Schiffbauer, J.D., Sun, B., Yuan, X., 2014. Tube growth patterns and microbial mat-related
726 lifestyles in the Ediacaran fossil Cloudina, Gaojiashan Lagerstätte, South China. Gondwana Research,
727 25(3): 1008-1018, doi:10.1016/j.gr.2012.12.027
728 Cai, Y., Hua, H., Xiao, S., Schiffbauer, J.D., Li, P., 2010. Biostratinomy of the late Ediacaran pyritized
729 Gaojiashan Lagerstätte from southern Shaanxi, South China: importance of event deposits. PALAIOS,
730 25(8): 487-506, doi:10.2110/palo.2009.p09-133r
731 Cai, Y., Schiffbauer, J.D., Hua, H., Xiao, S., 2011. Morphology and paleoecology of the late Ediacaran tubular
732 fossil Conotubus hemiannulatus from the Gaojiashan Lagerstätte of southern Shaanxi Province, South
733 China. Precambrian Research, 191(1): 46-57, doi:10.1016/j.precamres.2011.09.002
734 Calver, C.R., 2000. Isotope stratigraphy of the Ediacarian (Neoproterozoic III) of the Adelaide Rift Complex,
735 Australia, and the overprint of water column stratification. Precambrian Research, 100(1–3): 121-150,
736 doi:10.1016/s0301-9268(99)00072-8
737 Canfield, D.E., 2004. The evolution of the Earth surface sulfur reservoir. American Journal of Science,
738 304(10): 839-861, doi:10.2475/ajs.304.10.839
739 Canfield, D.E., Farquhar, J., 2009. Animal evolution, bioturbation, and the sulfate concentration of the oceans.
740 Proceedings of the National Academy of Sciences, 106(20): 8123-8127,
741 doi:10.1073/pnas.0902037106
742 Canfield, D.E., Farquhar, J., Zerkle, A.L., 2010. High isotope fractionations during sulfate reduction in a low-
743 sulfate euxinic ocean analog. Geology, 38(5): 415-418, doi:10.1130/G30723.1
744 Canfield, D.E., Thamdrup, B., 1994. The production of 34S-depleted sulfide during bacterial
745 disproportionation of elemental sulfur. Science, 266(5193): 1973-1975, doi:10.1126/science.11540246
746 Carbone, C., Narbonne, G.M., 2014. When life got smart: the evolution of behavioral complexity through the
747 Ediacaran and early Cambrian of NW Canada. Journal of Paleontology, 88(2): 309-330,
748 doi:10.1666/13-066
749 Chen, D., Zhou, X., Fu, Y., Wang, J., Yan, D., 2015. New U–Pb zircon ages of the Ediacaran–Cambrian
750 boundary strata in South China. Terra Nova, 27(1): 62-68, doi:10.1111/ter.12134
751 Chen, Z., Zhou, C., Meyer, M., Xiang, K., Schiffbauer, J.D., Yuan, X., Xiao, S., 2013. Trace fossil evidence
752 for Ediacaran bilaterian animals with complex behaviors. Precambrian Research, 224: 690-701,
753 doi:10.1016/j.precamres.2012.11.004
754 Chen, Z., Zhou, C., Xiao, S., Wang, W., Guan, C., Hua, H., Yuan, X., 2014a. New Ediacara fossils preserved
755 in marine limestone and their ecological implications. Scientific Reports, 4: 4180;
756 DOI:10.1038/srep04180
757 Chen, Z., Zhou, C., Xiao, S., Wang, W., Guan, C., Hua, H., Yuan, X., 2014b. New Ediacara fossils preserved
758 in marine limestone and their ecological implications. Scientific Reports, 4(4180),
759 doi:10.1038/srep04180
760 Condon, D., Zhu, M., Bowring, S., Wang, W., Yang, A., Jin, Y., 2005. U-Pb ages from the Neoproterozoic
761 Doushantuo Formation, China. Science, 308: 95-98
762 Conway Morris, S., Mattes, B.W., Chen, M., 1990. The early skeletal organism *Cloudina*: New occurrences
763 from Oman and possibly China. American Journal of Science, 290-A: 245-260
764 Cortijo, I., Cai, Y., Hua, H., Schiffbauer, J.D., Xiao, S., 2015. Life history and autecology of an Ediacaran
765 index fossil: Development and dispersal of Cloudina. Gondwana Research, 28: 419-424,
766 doi:10.1016/j.gr.2014.05.001

767 Cortijo, I., Martí Mus, M., Jensen, S., Palacios, T., 2010. A new species of Cloudina from the terminal
768 Ediacaran of Spain. Precambrian Research, 176(1–4): 1-10, doi:10.1016/j.precamres.2009.10.010
769 Cui, H., Kaufman, A.J., Xiao, S., Zhu, M., Zhou, C., Liu, X.-M., 2015. Redox architecture of an Ediacaran
770 ocean margin: Integrated chemostratigraphic (δ13C–δ34S–87Sr/86Sr–Ce/Ce*) correlation of the
771 Doushantuo Formation, South China. Chemical Geology, 405: 48-62,
772 doi:10.1016/j.chemgeo.2015.04.009
773 De La Rocha, C., DePaolo, D.J., 2000. Isotopic evidence for variations in the marine calcium cycle over the
774 Cenozoic. Science, 289(5482): 1176-1178, doi:10.1126/science.289.5482.1176
775 DePaolo, D.J., 2004. Calcium isotopic variations produced by biological, kinetic, radiogenic and
776 nucleosynthetic processes. Reviews in Mineralogy and Geochemistry, 55(1): 255-288,
777 doi:10.2138/gsrmg.55.1.255
778 DePaolo, D.J., 2011. Surface kinetic model for isotopic and trace element fractionation during precipitation of
779 calcite from aqueous solutions. Geochimica et Cosmochimica Acta, 75(4): 1039-1056,
780 doi:10.1016/j.gca.2010.11.020
781 Derry, L.A., 2010. A burial diagenesis origin for the Ediacaran Shuram-Wonoka carbon isotope anomaly.
782 Earth and Planetary Science Letters, 294(1–2): 152-162, doi:10.1016/j.epsl.2010.03.022
783 Des Marais, D.J., 1990. Microbial mats and the early evolution of life. Trends in Ecology & Evolution, 5(5):
784 140-144, doi:10.1016/0169-5347(90)90219-4
785 Duda, J.-P., Blumenberg, M., Thiel, V., Simon, K., Zhu, M., Reitner, J., 2014. Geobiology of a
786 palaeoecosystem with Ediacara-type fossils: The Shibantan Member (Dengying Formation, South
787 China). Precambrian Research, 255, Part 1(0): 48-62, doi:10.1016/j.precamres.2014.09.012
788 Duda, J.-P., Zhu, M., Reitner, J., 2015. Depositional dynamics of a bituminous carbonate facies in a
789 tectonically induced intra-platform basin: the Shibantan Member (Dengying Formation, Ediacaran
790 Period). Carbonates and Evaporites: 1-13, doi:10.1007/s13146-015-0243-8
791 Erwin, D.H., 2015. A public goods approach to major evolutionary innovations. Geobiology, 13(4): 308-315,
792 doi:10.1111/gbi.12137
793 Falkowski, P.G., Fenchel, T., Delong, E.F., 2008. The microbial engines that drive Earth's biogeochemical
794 cycles. Science, 320(5879): 1034-1039, doi:10.1126/science.1153213
795 Fike, D.A., Finke, N., Zha, J., Blake, G., Hoehler, T.M., Orphan, V.J., 2009. The effect of sulfate
796 concentration on (sub) millimeter-scale sulfide $\delta^{34}S$ in hypersaline cyanobacterial mats over the
797 diurnal cycle. Geochimica et Cosmochimica Acta, 73(20): 6187-6204, doi:10.1016/j.gca.2009.07.006
798 Fike, D.A., Gammon, C.L., Ziebis, W., Orphan, V.J., 2008. Micron-scale mapping of sulfur cycling across the
799 oxycline of a cyanobacterial mat: a paired nanoSIMS and CARD-FISH approach. The ISME journal,
800 2(7): 749-759, doi:10.1038/ismej.2008.39
801 Fike, D.A., Grotzinger, J.P., 2008. A paired sulfate-pyrite $\delta^{34}S$ approach to understanding the evolution of the
802 Ediacaran-Cambrian sulfur cycle. Geochem. Cosmochim. Acta, 72: 2636-2648,
803 doi:10.1016/j.gca.2008.03.021
804 Fike, D.A., Grotzinger, J.P., 2010. A $\delta^{34}S_{SO4}$ approach to reconstructing biogenic pyrite burial in carbonate-
805 evaporite basins: An example from the Ara Group, Sultanate of Oman. Geology, 38(4): 371-374,
806 doi:10.1130/g30230.1
807 Fike, D.A., Grotzinger, J.P., Pratt, L.M., Summons, R.E., 2006. Oxidation of the Ediacaran Ocean. Nature, 444:
808 744-747, doi:10.1038/nature05345
809 Gaidos, E., Dubuc, T., Dunford, M., McAndrew, P., Padilla-GamiÑO, J., Studer, B., Weersing, K., Stanley, S.,
810 2007. The Precambrian emergence of animal life: a geobiological perspective. Geobiology, 5(4): 351-
811 373, doi:10.1111/j.1472-4669.2007.00125.x
812 Gaucher, C., Germs, G.J.B., 2009. Skeletonised Metazoans and Protists. In: Gaucher, C., Sial, A.N., Frimmel,
813 H.E., Halverson, G.P. (Eds.), Developments in Precambrian Geology. Elsevier, pp. 327-338,
814 doi:10.1016/S0166-2635(09)01623-5
815 Gehling, J.G., 1999. Microbial mats in terminal Proterozoic siliciclastics: Ediacaran death masks. Palaios,
816 14(1): 40-57, doi:10.2307/3515360
817 Gehrels, G.E., Valencia, V.A., Ruiz, J., 2008. Enhanced precision, accuracy, efficiency, and spatial resolution
818 of U-Pb ages by laser ablation–multicollector–inductively coupled plasma–mass spectrometry.
819 Geochemistry, Geophysics, Geosystems, 9(3): Q03017, doi:10.1029/2007GC001805

820 Gill, B.C., Lyons, T.W., Frank, T.D., 2008. Behavior of carbonate-associated sulfate during meteoric
821 diagenesis and implications for the sulfur isotope paleoproxy. Geochimica et Cosmochimica Acta,
822 72(19): 4699-4711, doi:10.1016/j.gca.2008.07.001
823 Gingras, M., Konhauser, K., 2015. Digging deeper. Nature Geosci, 8: 825-826, doi:10.1038/ngeo2548
824 Gomes, M.L., Hurtgen, M.T., 2015. Sulfur isotope fractionation in modern euxinic systems: Implications for
825 paleoenvironmental reconstructions of paired sulfate–sulfide isotope records. Geochimica et
826 Cosmochimica Acta, 157: 39-55, doi:10.1016/j.gca.2015.02.031
827 Grant, S., 1990. Shell structure and distribution of Cloudina, a potential index fossil for the terminal
828 Proterozoic. American Journal of Science, 290: 261-294
829 Grant, S.W.F., 1992. Carbon isotopic vital effect and organic diagenesis, Lower Cambrian Forteau Formation,
830 northwest Newfoundland: Implications for δ13C chemostratigraphy. Geology, 20(3): 243-246,
831 doi:10.1130/0091-7613(1992)020<0243:civeao>2.3.co;2
832 Grotzinger, J., Adams, E., Schröder, S., 2005. Microbial-metazoan reefs of the terminal Proterozoic Nama
833 Group (c. 550-543 Ma), Namibia. Geological Magazine, 142(05): 499-517,
834 doi:10.1017/S0016756805000907
835 Grotzinger, J.P., 2000. Facies and paleoenvironmental setting of thrombolite-stromatolite reefs, terminal
836 Proterozoic Nama Group (ca. 550-543 Ma), central and southern Namibia. Communications of the
837 Geological Survey of Namibia, 12: 251-264
838 Grotzinger, J.P., Fike, D.A., Fischer, W.W., 2011. Enigmatic origin of the largest-known carbon isotope
839 excursion in Earth's history. Nature Geoscience, 4(5): 285-292, doi:10.1038/NGEO1138
840 Habicht, K.S., Canfield, D.E., 2001. Isotope fractionation by sulfate-reducing natural populations and the
841 isotopic composition of sulfide in marine sediments. Geology, 29(6): 555-558, doi:10.1130/0091-
842 7613(2001)029<0555:IFBSRN>2.0.CO;2
843 Habicht, K.S., Gade, M., Thamdrup, B., Berg, P., Canfield, D.E., 2002. Calibration of sulfate levels in the
844 Archean ocean. Science, 298(5602): 2372-2374, doi:10.1126/science.1078265
845 Hall, M., Kaufman, A.J., Vickers-Rich, P., Ivantsov, A., Trusler, P., Linnemann, U., Hofmann, M., Elliott, D.,
846 Cui, H., Fedonkin, M., Hoffmann, K.-H., Wilson, S.A., Schneider, G., Smith, J., 2013. Stratigraphy,
847 palaeontology and geochemistry of the late Neoproterozoic Aar Member, southwest Namibia:
848 Reflecting environmental controls on Ediacara fossil preservation during the terminal Proterozoic in
849 African Gondwana. Precambrian Research, 238: 214-232, doi:10.1016/j.precamres.2013.09.009
850 Halverson, G.P., Dudás, F.Ö., Maloof, A.C., Bowring, S.A., 2007. Evolution of the 87Sr/86Sr composition of
851 Neoproterozoic seawater. Palaeogeography, Palaeoclimatology, Palaeoecology, 256(3–4): 103-129,
852 doi:10.1016/j.palaeo.2007.02.028
853 Halverson, G.P., Hurtgen, M.T., 2007. Ediacaran growth of the marine sulfate reservoir. Earth and Planetary
854 Science Letters, 263(1): 32-44, doi:10.1016/j.epsl.2007.08.022
855 Hayes, J., Wedeking, K., Kaplan, I., 1983. Precambrian organic geochemistry-Preservation of the record. In:
856 Schopf, J.W. (Ed.), Earth's earliest biosphere: Its origin and evolution. Princeton University Press,
857 Princeton, NJ,, pp. 93-134
858 Hayes, J.M., 1993. Factors controlling ^{13}C contents of sedimentary organic compounds: Principles and
859 evidence. Marine Geology, 113(1–2): 111-125, doi:10.1016/0025-3227(93)90153-M
860 Higgins, J., Fischer, W., Schrag, D., 2009. Oxygenation of the ocean and sediments: consequences for the
861 seafloor carbonate factory. Earth and Planetary Science Letters, 284(1): 25-33,
862 doi:10.1016/j.epsl.2009.03.039
863 Higgins, J.A., Schrag, D.P., 2003. Aftermath of a snowball Earth. Geochemistry, Geophysics, Geosystems,
864 4(3): 1028, doi:10.1029/2002GC000403
865 Hoffman, P.F., Schrag, D.P., 2002. The snowball Earth hypothesis: testing the limits of global change. Terra
866 Nova, 14(3): 129-155, doi:10.1046/j.1365-3121.2002.00408.x
867 Houghton, J., Fike, D., Druschel, G., Orphan, V., Hoehler, T.M., Des Marais, D.J., 2014. Spatial variability in
868 photosynthetic and heterotrophic activity drives localized δ13Corg fluctuations and carbonate
869 precipitation in hypersaline microbial mats. Geobiology, 12(6): 557-574, doi:10.1111/gbi.12113
870 Hua, H., Chen, Z., Yuan, X., 2007. The advent of mineralized skeletons in Neoproterozoic Metazoa—new
871 fossil evidence from the Gaojiashan Fauna. Geological Journal, 42(3-4): 263-279, doi:10.1002/gj.1077

Hua, H., Chen, Z., Yuan, X., Zhang, L., Xiao, S., 2005. Skeletogenesis and asexual reproduction in the earliest biomineralizing animal Cloudina. Geology, 33(4): 277-280, doi:10.1130/g21198.1

Hua, H., Pratt, B.R., Zhang, L.-Y., 2003. Borings in Cloudina shells: complex predator-prey dynamics in the terminal Neoproterozoic. Palaios, 18(4-5): 454-459, doi:10.1669/0883-1351(2003)018<0454:BICSCP>2.0.CO;2

Hurtgen, M.T., Arthur, M.A., Halverson, G.P., 2005. Neoproterozoic sulfur isotopes, the evolution of microbial sulfur species, and the burial efficiency of sulfide as sedimentary pyrite. Geology, 33(1): 41-44, doi:10.1130/g20923.1

Jacobsen, S.B., Kaufman, A.J., 1999. The Sr, C and O isotopic evolution of Neoproterozoic seawater. Chemical Geology, 161(1–3): 37-57, doi:10.1016/s0009-2541(99)00080-7

Jiang, G., Kaufman, A.J., Christie-Blick, N., Zhang, S., Wu, H., 2007. Carbon isotope variability across the Ediacaran Yangtze platform in South China: Implications for a large surface-to-deep ocean $\delta^{13}C$ gradient. Earth and Planetary Science Letters, 261: 303-320, doi:10.1016/j.epsl.2007.07.009

Jiang, G., Shi, X., Zhang, S., Wang, Y., Xiao, S., 2011. Stratigraphy and paleogeography of the Ediacaran Doushantuo Formation (ca. 635–551Ma) in South China. Gondwana Research, 19(4): 831-849, doi:10.1016/j.gr.2011.01.006

Johnston, D.T., Wolfe-Simon, F., Pearson, A., Knoll, A.H., 2009. Anoxygenic photosynthesis modulated Proterozoic oxygen and sustained Earth's middle age. Proceedings of the National Academy of Sciences, 106(40): 16925-16929, doi:10.1073/pnas.0909248106

Jørgensen, B.B., Böttcher, M.E., Lüschen, H., Neretin, L.N., Volkov, I.I., 2004. Anaerobic methane oxidation and a deep H_2S sink generate isotopically heavy sulfides in Black Sea sediments 1. Geochimica et Cosmochimica Acta, 68(9): 2095-2118, doi:10.1016/j.gca.2003.07.017

Kah, L.C., Lyons, T.W., Frank, T.D., 2004. Low marine sulphate and protracted oxygenation of the Proterozoic biosphere. Nature, 431(7010): 834-838, doi:10.1038/nature02974

Katz, A., Sass, E., Starinsky, A., Holland, H., 1972. Strontium behavior in the aragonite-calcite transformation: an experimental study at 40–98°C. Geochimica et Cosmochimica Acta, 36(4): 481-496, doi:10.1016/0016-7037(72)90037-3

Kaufman, A.J., 2005. The calibration of Ediacaran time. Science, 308(5718): 59-60, doi:10.1126/science.1111101

Kaufman, A.J., Corsetti, F.A., Varni, M.A., 2007. The effect of rising atmospheric oxygen on carbon and sulfur isotope anomalies in the Neoproterozoic Johnnie Formation, Death Valley, USA. Chemical Geology, 237: 47-63, doi:10.1016/j.chemgeo.2006.06.023

Kaufman, A.J., Hayes, J.M., Knoll, A.H., Germs, G.J.B., 1991. Isotopic compositions of carbonates and organic carbon from upper Proterozoic successions in Namibia: stratigraphic variation and the effects of diagenesis and metamorphism. Precambrian Research, 49(3–4): 301-327, doi:10.1016/0301-9268(91)90039-D

Kaufman, A.J., Jacobsen, S.B., Knoll, A.H., 1993. The Vendian record of Sr and C isotopic variations in seawater: implications for tectonics and paleoclimate. Earth and Planetary Science Letters, 120(3): 409-430, doi:10.1016/0012-821X(93)90254-7

Kaufman, A.J., Jiang, G., Christie-Blick, N., Banerjee, D., Rai, V., 2006. Stable isotope record of the terminal Neoproterozoic Krol platform in the Lesser Himalayas of northern India. Precambrian Research, 147: 156-185, doi:10.1016/j.precamres.2006.02.007

Kaufman, A.J., Knoll, A.H., Narbonne, G.M., 1997. Isotopes, ice ages, and terminal Proterozoic earth history. Proceedings of the National Academy of Sciences, 94(13): 6600-6605

Kempe, S., Kazmierczak, J., Degens, E.T., 1989. The soda ocean concept and its bearing on biotic evolution. In: Crick, R.E. (Ed.), Origin, Evolution, and Modern Aspects of Biomineralization in Plants and Animals. Plenum Press, New York, pp. 29-43, doi:10.1007/978-1-4757-6114-6_3

Knauth, L.P., Kennedy, M.J., 2009. The late Precambrian greening of the Earth. Nature, 460: 728-732, doi:10.1038/nature08213

Knoll, A.H., 2003a. Biomineralization and evolutionary history, Reviews in mineralogy and geochemistry, pp. 329-356, doi:10.2113/0540329

Knoll, A.H., 2003b. The geological consequences of evolution. Geobiology, 1(1): 3-14, doi:10.1046/j.1472-4669.2003.00002.x

Knoll, A.H., Fischer, W.W., 2011. Skeletons and ocean chemistry: The long view. In: Gattuso, J.-P., Hansson, L. (Eds.), Ocean Acidification. Oxford University Press, New York, pp. 67-82

Kump, L., Arthur, M., Patzkowsky, M., Gibbs, M., Pinkus, D., Sheehan, P., 1999. A weathering hypothesis for glaciation at high atmospheric pCO_2 during the Late Ordovician. Palaeogeography, Palaeoclimatology, Palaeoecology, 152: 173-187, doi:10.1016/S0031-0182(99)00046-2

Leavitt, W.D., 2014. On the mechanisms of sulfur isotope fractionation during microbial sulfate reduction. Dissertation

Leavitt, W.D., Bradley, A.S., Halevy, I., Johnston, D.T., 2013. Influence of sulfate reduction rates on the Phanerozoic sulfur isotope record. Proc. Natl Acad. Sci. USA, 110: 11244-11249

Lenton, T.M., Boyle, R.A., Poulton, S.W., Shields-Zhou, G.A., Butterfield, N.J., 2014. Co-evolution of eukaryotes and ocean oxygenation in the Neoproterozoic era. Nature Geoscience, 7: 257–265, doi:10.1038/ngeo2108

Li, C., Love, G.D., Lyons, T.W., Fike, D.A., Sessions, A.L., Chu, X., 2010. A stratified redox model for the Ediacaran ocean. Science, 328(5974): 80-83, doi:10.1126/science.1182369

Ling, H.-F., Chen, X., Li, D., Wang, D., Shields-Zhou, G.A., Zhu, M., 2013. Cerium anomaly variations in Ediacaran–earliest Cambrian carbonates from the Yangtze Gorges area, South China: Implications for oxygenation of coeval shallow seawater. Precambrian Research, 225: 110-127, doi:10.1016/j.precamres.2011.10.011

Liu, X.-M., Kah, L.C., Knoll, A.H., Cui, H., Kaufman, A.J., Shahar, A., Hazen, R.M., 2016. Tracing Earth's O_2 evolution using Zn/Fe ratios in marine carbonates. Geochemical Perspectives Letters, 2: 24-34, doi:10.7185/geochemlet.1603

Lorens, R.B., 1981. Sr, Cd, Mn and Co distribution coefficients in calcite as a function of calcite precipitation rate. Geochimica et Cosmochimica Acta, 45(4): 553-561, doi:10.1016/0016-7037(81)90188-5

Loyd, S.J., Marenco, P.J., Hagadorn, J.W., Lyons, T.W., Kaufman, A.J., Sour-Tovar, F., Corsetti, F.A., 2013. Local $\delta^{34}S$ variability in ~580Ma carbonates of northwestern Mexico and the Neoproterozoic marine sulfate reservoir. Precambrian Research, 224: 551-569, doi:10.1016/j.precamres.2012.10.007

Lu, M., Zhu, M., Zhang, J., Shields-Zhou, G., Li, G., Zhao, F., Zhao, X., Zhao, M., 2013. The DOUNCE event at the top of the Ediacaran Doushantuo Formation, South China: Broad stratigraphic occurrence and non-diagenetic origin. Precambrian Research, 225: 86-109, doi:10.1016/j.precamres.2011.10.018

Ludwig, K., 2008. Isoplot 3.6, Berkeley Geochronology Center Special Publication 4. 77

Lyons, T.W., Reinhard, C.T., Planavsky, N.J., 2014. The rise of oxygen in Earth's early ocean and atmosphere. Nature, 506(7488): 307-315, doi:10.1038/nature13068

Lyons, T.W., Walter, L.M., Gellatly, A.M., Martini, A.M., Blake, R.E., 2004. Sites of anomalous organic remineralization in the carbonate sediments of South Florida, USA: the sulfur cycle and carbonate-associated sulfate. Geological Society of America Special Papers, 379: 161-176, doi:10.1130/0-8137-2379-5.161

Marenco, P.J., Corsetti, F.A., Hammond, D.E., Kaufman, A.J., Bottjer, D.J., 2008. Oxidation of pyrite during extraction of carbonate associated sulfate. Chemical Geology, 247(1–2): 124-132, doi:10.1016/j.chemgeo.2007.10.006

Martin, A.J., Southworth, S., Collins, J.C., Fisher, S.W., Kingman, E.R., 2015. Laurentian and Amazonian sediment sources to Neoproterozoic–lower Paleozoic Maryland Piedmont rocks. Geosphere, 11(4): 1042-1061, doi:10.1130/GES01140.1

Mazumdar, A., Strauss, H., 2006. Sulfur and strontium isotopic compositions of carbonate and evaporite rocks from the late Neoproterozoic–early Cambrian Bilara Group (Nagaur-Ganganagar Basin, India): Constraints on intrabasinal correlation and global sulfur cycle. Precambrian Research, 149(3–4): 217-230, doi:10.1016/j.precamres.2006.06.008

McArthur, J., Howarth, R., Shields, G., 2012. Strontium isotope stratigraphy. In: Gradstein, F.M., Ogg, J.G., Schmitz, M.D., Ogg, G.M. (Eds.), The Geologic Time Scale 2012. Elsevier B.V, pp. 127-144, doi:10.1016/B978-0-444-59425-9.00007-X

McFadden, K.A., Huang, J., Chu, X., Jiang, G., Kaufman, A.J., Zhou, C., Yuan, X., Xiao, S., 2008. Pulsed oxidation and biological evolution in the Ediacaran Doushantuo Formation. Proceedings of the National Academy of Sciences, 105(9): 3197-3202, doi:10.1073/pnas.0708336105

Melezhik, V.A., Pokrovsky, B.G., Fallick, A.E., Kuznetsov, A.B., Bujakaite, M.I., 2009. Constraints on $^{87}Sr/^{86}Sr$ of Late Ediacaran seawater: insight from Siberian high-Sr limestones. Journal of the Geological Society, 166(1): 183-191, doi:10.1144/0016-76492007-171

Meyer, M., Schiffbauer, J.D., Xiao, S., Cai, Y., Hua, H., 2012. Taphonomy of the upper Ediacaran enigmatic ribbonlike fossil *Shaanxilithes*. PALAIOS, 27(5): 354-372, doi:10.2110/palo.2011.p11-098r

Meyer, M., Xiao, S., Gill, B.C., Schiffbauer, J.D., Chen, Z., Zhou, C., Yuan, X., 2014. Interactions between Ediacaran animals and microbial mats: Insights from Lamonte trevallis, a new trace fossil from the Dengying Formation of South China. Palaeogeography, Palaeoclimatology, Palaeoecology, 396: 62-74, doi:10.1016/j.palaeo.2013.12.026

Meysman, F.J., Middelburg, J.J., Heip, C.H., 2006. Bioturbation: a fresh look at Darwin's last idea. Trends in Ecology & Evolution, 21(12): 688-695, doi:10.1016/j.tree.2006.08.002

Nielsen, L.C., Druhan, J.L., Yang, W., Brown, S.T., DePaolo, D.J., 2011. Calcium isotopes as tracers of biogeochemical processes. In: Baskaran, M. (Ed.), Handbook of Environmental Isotope Geochemistry. Springer-Verlag Berlin Heidelberg, pp. 105-124, doi:10.1007/978-3-642-10637-8_7

Och, L.M., Shields-Zhou, G.A., 2012. The Neoproterozoic oxygenation event: Environmental perturbations and biogeochemical cycling. Earth-Science Reviews, 110(1–4): 26-57, doi:10.1016/j.earscirev.2011.09.004

Paris, G., Adkins, J., Sessions, A., Webb, S., Fischer, W., 2014. Neoarchean carbonate–associated sulfate records positive $\Delta^{33}S$ anomalies. Science, 346(6210): 739-741, doi:10.1126/science.1258211

Peng, Y., Bao Huiming, P.M.L., Kaufman J. Alan, Jiang Ganqing, Boyd Dustin, Wang Qinxian, Zhou Chuanming, Yuan Xunlai, Xiao Shuhai, Sean, L., 2014. Widespread contamination of carbonate-associated sulfate by present-day secondary atmospheric sulfate: evidence from triple oxygen isotopes. Geology, 42(9): 815-818, doi:10.1130/G35852.1

Penny, A., Wood, R., Curtis, A., Bowyer, F., Tostevin, R., Hoffman, K.-H., 2014. Ediacaran metazoan reefs from the Nama Group, Namibia. Science, 344(6191): 1504-1506, doi:10.1126/science.1253393

Porter, S., 2011. The rise of predators. Geology, 39(6): 607-608, doi:10.1130/focus062011.1

Porter, S.M., 2007. Seawater chemistry and early carbonate biomineralization. Science, 316(5829): 1302-1302

Porter, S.M., 2010. Calcite and aragonite seas and the de novo acquisition of carbonate skeletons. Geobiology, 8(4): 256-277, doi:10.1111/j.1472-4669.2010.00246.x

Reuschel, M., Melezhik, V., Whitehouse, M., Lepland, A., Fallick, A., Strauss, H., 2012. Isotopic evidence for a sizeable seawater sulfate reservoir at 2.1 Ga. Precambrian Research, 192: 78-88, doi:10.1016/j.precamres.2011.10.013

Ries, J.B., Fike, D.A., Pratt, L.M., Lyons, T.W., Grotzinger, J.P., 2009. Superheavy pyrite ($\delta^{34}S_{pyr}>\delta^{34}S_{CAS}$) in the terminal Proterozoic Nama Group, southern Namibia: A consequence of low seawater sulfate at the dawn of animal life. Geology, 37(8): 743-746, doi:10.1130/g25775a.1

Rogov, V., Marusin, V., Bykova, N., Goy, Y., Nagovitsin, K., Kochnev, B., Karlova, G., Grazhdankin, D., 2012. The oldest evidence of bioturbation on Earth. Geology, 40(5): 395-398

Sahoo, S.K., Planavsky, N.J., Kendall, B., Wang, X., Shi, X., Scott, C., Anbar, A.D., Lyons, T.W., Jiang, G., 2012. Ocean oxygenation in the wake of the Marinoan glaciation. Nature, 489(7417): 546-549, doi:10.1038/nature11445

Sawaki, Y., Ohno, T., Tahata, M., Komiya, T., Hirata, T., Maruyama, S., Windley, B.F., Han, J., Shu, D., Li, Y., 2010. The Ediacaran radiogenic Sr isotope excursion in the Doushantuo Formation in the Three Gorges area, South China. Precambrian Research, 176(1–4): 46-64, doi:10.1016/j.precamres.2009.10.006

Sawaki, Y., Tahata, M., Ohno, T., Komiya, T., Hirata, T., Maruyama, S., Han, J., Shu, D., 2014. The anomalous Ca cycle in the Ediacaran ocean: evidence from Ca isotopes preserved in carbonates in the Three Gorges area, South China. Gondwana Research, 25(3): 1070-1089, doi:10.1016/j.gr.2013.03.008

Saylor, B.Z., Kaufman, A.J., Grotzinger, J.P., Urban, F., 1998. A composite reference section for terminal Proterozoic strata of southern Namibia. Journal of Sedimentary Research, 68(6): 1223-1235, doi:10.2110/jsr.68.1223

1028 Schiffbauer, J.D., Xiao, S., Cai, Y., Wallace, A.F., Hua, H., Hunter, J., Xu, H., Peng, Y., Kaufman, A.J., 2014.
1029 A unifying model for Neoproterozoic–Palaeozoic exceptional fossil preservation through pyritization
1030 and carbonaceous compression. Nature Communications, 5: 5754, doi:10.1038/ncomms6754
1031 Schobben, M., Stebbins, A., Ghaderi, A., Strauss, H., Korn, D., Korte, C., 2015. Flourishing ocean drives the
1032 end-Permian marine mass extinction. Proceedings of the National Academy of Sciences, 112(33):
1033 10298-10303, doi:10.1073/pnas.1503755112
1034 Schrag, D.P., Higgins, J.A., Macdonald, F.A., Johnston, D.T., 2013. Authigenic carbonate and the history of
1035 the global carbon cycle. Science, 339(6119): 540-543, doi:10.1126/science.1229578
1036 Seilacher, A., Pflüger, F., 1994. From biomats to benthic agriculture: a biohistoric revolution. Biostabilization
1037 of sediments: 97-105
1038 Shen, B., Xiao, S., Bao, H., Kaufman, A.J., Zhou, C., Yuan, X., 2011. Carbon, sulfur, and oxygen isotope
1039 evidence for a strong depth gradient and oceanic oxidation after the Ediacaran Hankalchough
1040 glaciation. Geochimica et Cosmochimica Acta, 75(5): 1357-1373, doi:10.1016/j.gca.2010.12.015
1041 Shen, B., Xiao, S., Kaufman, A.J., Bao, H., Zhou, C., Wang, H., 2008. Stratification and mixing of a post-
1042 glacial Neoproterozoic ocean: Evidence from carbon and sulfur isotopes in a cap dolostone from
1043 northwest China. Earth and Planetary Science Letters, 265(1–2): 209-228,
1044 doi:10.1016/j.epsl.2007.10.005
1045 Shen, B., Xiao, S., Zhou, C., Kaufman, A.J., Yuan, X., 2010. Carbon and sulfur isotope chemostratigraphy of
1046 the Neoproterozoic Quanji Group of the Chaidam Basin, NW China: Basin stratification in the
1047 aftermath of an Ediacaran glaciation postdating the Shuram event? Precambrian Research, 177(3–4):
1048 241-252, doi:10.1016/j.precamres.2009.12.006
1049 Shen, Y., Canfield, D.E., Knoll, A.H., 2002. Middle Proterozoic ocean chemistry: Evidence from the
1050 McArthur Basin, northern Australia. American Journal of Science, 302(2): 81-109,
1051 doi:10.2475/ajs.302.2.81
1052 Shields-Zhou, G., Och, L., 2011. The case for a Neoproterozoic oxygenation event: geochemical evidence and
1053 biological consequences. GSA Today, 21(3): 4-11, doi:10.1130/GSATG102A.1
1054 Shields, G., 2007. A normalised seawater strontium isotope curve: possible implications for Neoproterozoic-
1055 Cambrian weathering rates and the further oxygenation of the Earth. eEarth, 2(2): 35-42,
1056 doi:10.5194/ee-2-35-2007
1057 Siegmund, H., Erdtmann, B.-D., 1994. Facies and diagenesis of some upper proterozoic dolomites of South
1058 China. Facies, 31(1): 255-263, doi:10.1007/BF02536942
1059 Sim, M.S., Bosak, T., Ono, S., 2011. Large sulfur isotope fractionation does not require disproportionation.
1060 Science, 333(6038): 74-77, doi:10.1126/science.1205103
1061 Simkiss, K., 1977. Biomineralization and detoxification. Calcified Tissue Research, 24(1): 199-200,
1062 doi:10.1007/BF02223316
1063 Simkiss, K., 1989. Biomineralisation in the context of geological time. Transactions of the Royal Society of
1064 Edinburgh: Earth Sciences, 80(3-4): 193-199, doi:10.1017/S0263593300028637
1065 Sour-Tovar, F., Hagadorn, J.W., Huitron-Rubio, T., 2007. Ediacaran and Cambrian index fossils from Sonora,
1066 Mexico. Palaeontology, 50(1): 169-175, doi:10.1111/j.1475-4983.2006.00619.x
1067 Stanley, S.M., 2006. Influence of seawater chemistry on biomineralization throughout Phanerozoic time:
1068 Paleontological and experimental evidence. Palaeogeography, Palaeoclimatology, Palaeoecology,
1069 232(2): 214-236, doi:10.1016/j.palaeo.2005.12.010
1070 Stanley, S.M., Hardie, L.A., 1998. Secular oscillations in the carbonate mineralogy of reef-building and
1071 sediment-producing organisms driven by tectonically forced shifts in seawater chemistry.
1072 Palaeogeography, Palaeoclimatology, Palaeoecology, 144(1): 3-19, doi:10.1016/S0031-
1073 0182(98)00109-6
1074 Steiner, M., Li, G., Qian, Y., Zhu, M., 2004. Lower Cambrian small shelly fossils of northern Sichuan and
1075 southern Shaanxi (China), and their biostratigraphic importance. Geobios, 37(2): 259-275,
1076 doi:10.1016/j.geobios.2003.08.001
1077 Stoll, H.M., Bains, S., 2003. Coccolith Sr/Ca records of productivity during the Paleocene-Eocene thermal
1078 maximum from the Weddell Sea. Paleoceanography, 18(2): 1049, doi:10.1029/2002PA000875

Stoll, H.M., Schrag, D.P., 2001. Sr/Ca variations in Cretaceous carbonates: relation to productivity and sea level changes. Palaeogeography, Palaeoclimatology, Palaeoecology, 168(3): 311-336, doi:10.1016/S0031-0182(01)00205-X

Strauss, H., Banerjee, D.M., Kumar, V., 2001. The sulfur isotopic composition of Neoproterozoic to early Cambrian seawater — evidence from the cyclic Hanseran evaporites, NW India. Chemical Geology, 175(1–2): 17-28, doi:10.1016/S0009-2541(00)00361-2

Tang, J., Köhler, S.J., Dietzel, M., 2008. Sr^{2+}/Ca^{2+} and $^{44}Ca/^{40}Ca$ fractionation during inorganic calcite formation: I. Sr incorporation. Geochimica et Cosmochimica Acta, 72(15): 3718-3732, doi:10.1016/j.gca.2008.05.031

Tarhan, L.G., Droser, M.L., 2014. Widespread delayed mixing in early to middle Cambrian marine shelfal settings. Palaeogeography, Palaeoclimatology, Palaeoecology, 399(0): 310-322, doi:10.1016/j.palaeo.2014.01.024

Tarhan, L.G., Droser, M.L., Planavsky, N.J., Johnston, D.T., 2015. Protracted development of bioturbation through the early Palaeozoic Era. Nature Geosci, 8: 865–869, doi:10.1038/ngeo2537

Tesoriero, A.J., Pankow, J.F., 1996. Solid solution partitioning of Sr^{2+}, Ba^{2+}, and Cd^{2+} to calcite. Geochimica et Cosmochimica Acta, 60(6): 1053-1063, doi:10.1016/0016-7037(95)00449-1

Wang, X., Jiang, G., Shi, X., Xiao, S., 2016. Paired carbonate and organic carbon isotope variations of the Ediacaran Doushantuo Formation from an upper slope section at Siduping, South China. Precambrian Research, 273: 53-66, doi:10.1016/j.precamres.2015.12.010

Weiner, S., Dove, P.M., 2003. An overview of biomineralization processes and the problem of the vital effect. Reviews in Mineralogy and Geochemistry, 54(1): 1-29

Wing, B.A., Halevy, I., 2014. Intracellular metabolite levels shape sulfur isotope fractionation during microbial sulfate respiration. Proceedings of the National Academy of Sciences, 111(51): 18116-18125, doi:10.1073/pnas.1407502111

Wood, R., Curtis, A., 2015. Extensive metazoan reefs from the Ediacaran Nama Group, Namibia: the rise of benthic suspension feeding. Geobiology, 13: 112-122, doi:10.1111/gbi.12122

Wood, R.A., Poulton, S.W., Prave, A.R., Hoffmann, K.H., Clarkson, M.O., Guilbaud, R., Lyne, J.W., Tostevin, R., Bowyer, F., Penny, A.M., Curtis, A., Kasemann, S.A., 2015. Dynamic redox conditions control late Ediacaran metazoan ecosystems in the Nama Group, Namibia. Precambrian Research, 261(0): 252-271, doi:10.1016/j.precamres.2015.02.004

Wotte, T., Shields-Zhou, G.A., Strauss, H., 2012. Carbonate-associated sulfate: Experimental comparisons of common extraction methods and recommendations toward a standard analytical protocol. Chemical Geology, 326–327: 132-144, doi:10.1016/j.chemgeo.2012.07.020

Wray, J.L., Daniels, F., 1957. Precipitation of calcite and aragonite. Journal of the American Chemical Society, 79(9): 2031-2034, doi:10.1021/ja01566a001

Wu, N., Farquhar, J., 2013. Metabolic rates and sulfur cycling in the geologic record. Proceedings of the National Academy of Sciences, 110(28): 11217-11218, doi:10.1073/pnas.1309726110

Wu, N., Farquhar, J., Fike, D.A., 2015. Ediacaran sulfur cycle: Insights from sulfur isotope measurements ($\Delta^{33}S$ and $\delta^{34}S$) on paired sulfate–pyrite in the Huqf Supergroup of Oman. Geochimica et Cosmochimica Acta, 164(0): 352-364, doi:10.1016/j.gca.2015.05.031

Xiao, S., 2014. Oxygen and early animal evolution. In: Turekian, K., Holland, H. (Eds.), Treatise on Geochemistry (Second Edition). Elsevier, Oxford, pp. 231-250, doi:10.1016/B978-0-08-095975-7.01310-3

Xiao, S., Schiffbauer, J.D., McFadden, K.A., Hunter, J., 2010. Petrographic and SIMS pyrite sulfur isotope analyses of Ediacaran chert nodules: Implications for microbial processes in pyrite rim formation, silicification, and exceptional fossil preservation. Earth and Planetary Science Letters, 297(3–4): 481-495, doi:10.1016/j.epsl.2010.07.001

Zhang, F., Kendall, B., Cui, H., Anbar, A.D., Xiao, S., Kaufman, A.J., 2015. An episode of widespread ocean anoxia during the latest Ediacaran Period revealed by light U isotope compositions in carbonates. GSA abstract

Zhelezinskaia, I., Kaufman, A.J., Farquhar, J., Cliff, J., 2014. Large sulfur isotope fractionations associated with Neoarchean microbial sulfate reduction. Science, 346(6210): 742-744, doi:10.1126/science.1256211

1132 Zhou, C., Xiao, S., 2007. Ediacaran $\delta^{13}C$ chemostratigraphy of South China. Chemical Geology, 237(1–2): 89-
1133 108, doi:10.1016/j.chemgeo.2006.06.021
1134 Zhu, M., Zhang, J., Yang, A., 2007. Integrated Ediacaran (Sinian) chronostratigraphy of South China.
1135 Palaeogeography, Palaeoclimatology, Palaeoecology, 254: 7-61, doi:10.1016/j.palaeo.2007.03.025
1136 Zhuravlev, A.Y., Liñán, E., Vintaned, J.A.G., Debrenne, F., Fedorov, A.B., 2012. New finds of skeletal fossils
1137 in the terminal Neoproterozoic of the Siberian Platform and Spain. Acta Palaeontologica Polonica,
1138 57(1): 205-224, doi:10.4202/app.2010.0074
1139 Zhuravlev, A.Y., Wood, R.A., Penny, A.M., 2015. Ediacaran skeletal metazoan interpreted as a lophophorate.
1140 Proceedings of the Royal Society of London B: Biological Sciences, 282: 20151860,
1141 doi:10.1098/rspb.2015.1860

1142

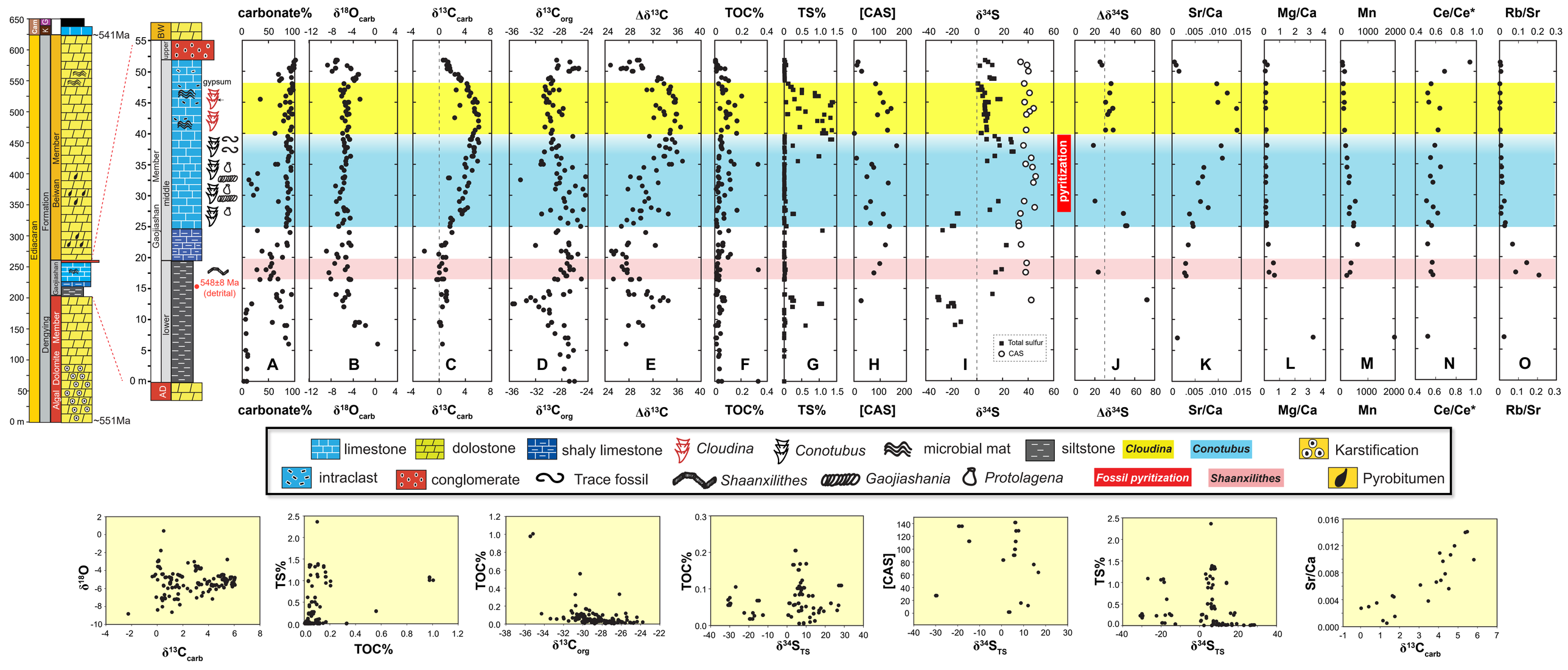
Cam
K
G
Ediacaran
Dengying Formation
Dolomite Member
Algal
Gaojiashan
Beiwan Member
~541Ma
~551Ma
650
600
550
500
450
400
350
300
250
200
150
100
50
0 m
BW
upper
Gaojiashan Member
middle
lower
AD
gypsum
548±8 Ma
(detrital)
55
50
45
40
35
30
25
20
15
10
5
0 m
carbonate%
δ18Ocarb
δ13Ccarb
δ13Corg
Δδ13C
TOC%
TS%
[CAS]
δ34S
Δδ34S
Sr/Ca
Mg/Ca
Mn
Ce/Ce*
Rb/Sr
pyritization
Total sulfur
CAS
A
B
C
D
E
F
G
H
I
J
K
L
M
N
O
limestone
dolostone
shaly limestone
Cloudina
Conotubus
microbial mat
siltstone
Cloudina
Conotubus
Karstification
intraclast
conglomerate
Trace fossil
Shaanxilithes
Gaojiashania
Protolagena
Fossil pyritization
Shaanxilithes
Pyrobitumen
δ18O
δ13Ccarb
TS%
TOC%
TOC%
δ13Corg
TOC%
δ34STS
[CAS]
δ34STS
TS%
δ34STS
Sr/Ca
δ13Ccarb